Human antibody C10 neutralizes by diminishing zika but enhancing dengue dynamics

Xin-Xiang Lim[1*], Bo Shu[2*], Shuijun Zhang[2*†], Aaron W.K. Tan[2], Thiam-Seng Ng[2], Xin-Ni Lim[2], Valerie S-Y Chew[2], Jian Shi[4], Gavin R. Screaton[3], Shee-Mei Lok[1,2,4©], Ganesh S. Anand[1,5©]

[1] Department of Biological Sciences, National University of Singapore, 14 Science Drive 4, Singapore 117543

[2]Duke-National University of Singapore Medical School, 8 College Road, Singapore 169857

[3]Medical Sciences Division, University of Oxford, Oxford OX3 9D

[4]Centre for Bioimaging Sciences, National University of Singapore, 14 Science Drive 4, Singapore 117557, Singapore

[5]Department of Chemistry, The Pennsylvania State University, 104 Chemistry Building, University Park, PA 16802, USA

†Current address: College of Life Sciences, Nanjing Agricultural University, Nanjing 210095,

China

Running Title: Fab C10 binding enhances conformational dynamics of DENV2 E-proteins but not ZIKV

Keywords: Non-uniform epitope recognition, intradimer contacts, DENV2 and ZIKV viral particle dynamics

*** Authors contributed equally to this work**

To whom correspondence should be addressed: ©Sheemei-Lok, [2]Duke-National University of Singapore Medical School, 8 College Road, Singapore 169857, phone: (65) 65165840 and email: sheemeilok@duke-nus.edu.sg

©Ganesh S. Anand, Department of Chemistry, The Pennsylvania State University, University Park, PA 16802 email: gsa5089@psu.edu

Summary

The human monoclonal antibody (HMAb) C10 potently cross-neutralizes zika (ZIKV) and dengue viruses. Analysis of Fab C10 interactions with both ZIKV and dengue serotype 2 (DENV2) particles by cryoEM and HDXMS show Fab C10 binding decreases overall ZIKV particle dynamics, whereas with DENV2, the same Fab causes increased dynamics. Testing of different Fab C10:DENV2 E protein molar ratios revealed that at higher Fab ratios, especially at saturated concentrations, the Fab enhanced viral dynamics (detected by HDXMS) and observation under cryoEM showed increased the number of distorted particles. Our results suggest that, Fab C10 stabilizes ZIKV, but with DENV2 particles, high Fab C10 occupancy promotes E protein dimer conformational changes leading to overall increased particle dynamics and distortion of the viral surface. This is a first instance of a broadly neutralizing antibody eliciting virus-specific increases in whole viral particle dynamics.

Introduction

Flavivirus infections are the most prevalent arthropod-borne diseases and represent a major global public health burden (Bhatt et al., 2013). Dengue (DENV) and Zika (ZIKV) viruses are two serious pathogens belonging to the *Flaviviridae* family (Westaway et al., 1985). There are four DENV serotypes and one serotype of ZIKV (Whitehead et al., 2007). The mature flavivirus virion is composed of a single-stranded RNA genome, 3 structural proteins: capsid (C), envelope (E) and membrane (M) proteins and a lipid bilayer membrane (Kuhn et al., 2002). The virus surface comprises 180 copies of E and M- protein heterodimers arranged with icosahedral symmetry (Zhang et al., 2013a; Kostyuchenko et al., 2016). The E-proteins exist as 90 E-protein dimers with the protomers oriented in an antiparallel head to tail fashion (Zhang et al., 2013a). Three parallel E-protein dimers (6 E-protein protomers) constitute a raft, and 30 rafts are arranged in a herringbone pattern to form the icosahedral virus surface (Zhang et al., 2013a). Each of the 60 asymmetric units are formed by three individual E proteins (molecules A, B and C) (Figure S1A). A raft consists of two asymmetric units containing three dimers (A/C', B/B' and C/A'). The A/C dimers [either (A/C', or C/A')] are hereafter referred to as L2 dimers, and the B/B' dimers, I2 dimers (Figure S1A), consistent with the accompanying paper (Sharma et al., 2021). Although the

overall conformation of the L2 and I2 dimers is the same, they have different local environments on the virus surface (Figure S1A) – one side of the L2 dimer is at the E-E inter-raft interface, and the other side E-E inter-dimer interface whereas, the I2 dimer is surrounded by inter-dimer interfaces. An E-protein consists of three ectodomains (DI, DII and DIII) (Modis et al., 2003) and is the major antigenic structure on the viral surface.

Previous studies using amide hydrogen/deuterium exchange mass spectrometry (HDXMS) and cryoEM showed that different serotypes and strains of DENV particles displayed varying magnitudes of intrinsic dynamics in solution (Lim et al., 2017b) with reversible or irreversible conformational fluctuations (Fibriansah et al., 2013; Zhang et al., 2013b) in response to an increase in temperature. This suggests flaviviruses are highly dynamic particles in solution and this property is critical for antibody recognition.

Recently, an important class of highly potent and broadly neutralizing E-dimer dependent epitope (EDE) antibodies were isolated from patients with mostly secondary dengue infections (Dejnirattisai et al., 2015). Interestingly, C10 also exhibited potent neutralization of Zika virus (Barba-Spaeth et al., 2016).

To uncover the basis for the broad neutralization of C10 with DENV and ZIKV, we set out to probe interactions of the Fab fragment of C10 with DENV2 NGC strain and ZIKV through an

integrated approach combining cryoEM and HDXMS. HDXMS offers a powerful thermodynamic readout of whole viral particles in solution (Lim et al., 2017a) using backbone amides as conformational probes for dynamics at peptide resolution in the millisecond and slower timescales (Englander and Kallenbach, 1983). HDXMS of dengue whole virus particles mapped viral surface breathing dynamic hotspots and temperature-dependent expansion (Lim et al., 2017a).

Here we report the effects of Fab C10 binding to ZIKV and DENV2 (NGC strain). Fab C10 at saturating concentrations decreased ZIKV dynamics, while increasing concentrations of Fab C10 induced overall increases in dynamics in DENV2. We observed at all Fab C10:E protein molar ratios (1:3, 2:3 and 3:3), Fab C10 shows a strong preference to bind L2 dimers over I2 dimers. At saturating Fab concentrations (3Fab:3E molar ratio), a subpopulation of viral particles becomes distorted, consistent with the increased E protein dynamics detected. The accompanying paper (Sharma et al., 2021), shows Fab C10 binding to DENV2 E protein ectodomain dimer can result in distortion of the dimeric conformation for DENV2 but not for ZIKV. Together, our results show that Fab when bound to DENV2 induce conformational changes in E protein, and at high Fab occupancies, this conformational change can lead to virus surface becoming distorted which is also corroborated by the increases in E protein dynamics. These results highlight the contrasting effects that the same Fab can have on the ZIKV and DENV2 surfaces.

Results

The neutralization mechanism of HMAb C10

Antibodies are capable of neutralizing viruses by various mechanisms; for instance, through inhibition of virus attachment to cells, or inhibition of virus:endosomal membrane fusion, or both. To investigate whether HMAb C10 can prevent virus binding to target cells, the IgG was mixed with DENV2 and then incubated with BHK-21 cells, that were precooled at 4 ℃. The unbound virus was then washed away and then real-time reverse transcription-PCR (RT-PCR) was used to quantify the remaining virus bound to the cells. The result shows that IgG at the concentrations tested (0.1 to 10 ug/ml) inhibited virus attachment to cells by ~50% to ~70% for both DENV2 and ZIKV (Figure 1A). This suggests that the antibody is able to partially block virus attachment to BHK-21 cells.

We previously have observed under cryoEM that for DENV, exposure to low pH (pH 5.0) caused virus aggregation. This is due to the individual virus particles fusing with each other, probably the result of E proteins flipping up at low pH, and then attaching to membranes of adjacent viral particles. This process mimics the structural changes necessary for fusion of DENV particles with the endosomal membrane at low pH. Therefore, we can use this assay to test if Fab C10 could block structural changes that are required for fusion. Fab C10 was first added to DENV2

115 at pH 8.0, which mimics the extracellular environment. We subsequently lowered the pH from 8.0
116 to either 6.5 (early endosome pH) or 5.0 (late endosome pH). The controls were uncomplexed
117 virus particles at the respective pH conditions. CryoEM micrographs of uncomplexed DENV2
118 particles at pH 8.0 showed mostly particles with a smooth surface. At pH 6.5, most uncomplexed
119 DENV2 particles were similar to those observed at pH 8.0, but some had undergone distortion. At
120 pH 5.0, the uncomplexed virus particles appeared smaller and spiky and had aggregated. When
121 Fab C10 was present, the virus particles did not aggregate under any of the above pH conditions,
122 suggesting that Fab C10 binding was capable of inhibiting fusion. (Figure 1B).

123 Overall, our results indicate that HMAb C10 can partially prevent virus attachment to cells
124 and inhibit virus-endosomal membrane fusion.

125 **Mapping Fab C10 complexes with ZIKV and DENV2 particles by HDXMS**

126 The C10 epitope has been previously mapped by cryoEM and X-ray crystallography
127 (Zhang et al., 2016; Rouvinski et al., 2015), however, those studies did not measure any viral
128 surface protein dynamics changes upon antibody binding. Here we use HDXMS to map the epitope
129 to peptide resolution and probe E protein surface dynamics (Lim et al., 2017a; Mandell et al.,
130 1998).

Interactions of Fabs on whole viral particles are influenced by the extensive E-E quaternary interactions on the whole virus. HDXMS will detect both the E-E protein intrinsic dynamics and also the antibody-binding induced changes in viral dynamics. In the rest of the manuscript, the whole DENV2 particle and the recombinant DENV2 E protein ectodomain are referred to as DENV2 and sE, respectively. Thus, HDXMS of the Fab C10:sE protein maps the C10 epitope on sE proteins, while that of Fab C10:DENV2 captures a combination of epitope interactions with any allosteric/long-range changes of the E protein conformation induced upon antibody binding.

Fab C10 binding decreases ZIKV surface dynamics by HDXMS

To map interactions of Fab C10 with ZIKV, we obtained 34 pepsin fragment peptides with high signal to noise and spanning 65.5% of ZIKV E-protein amino acid sequences (Figure S1B). Decreases in deuterium exchange were observed in peptides spanning residues 69-82 (*b* strand, *bc* loop), 90-107 (*c* strand, *cd* loop) and 243-269 (*ij* hairpin, α2 helix) (Figure 2A). These peptides spanned part of the C10 epitopes – including the fusion loop, identified from the cryoEM structure of Fab C10:ZIKV complex (Zhang et al., 2016).

On the antibody, we detected decreases in deuterium exchange in peptides spanning the heavy chain (residues 35-71, 94-106 and 116-123) and light chain (residues 19-32, 38-74 and 87-103) interfaces (Figures S2A, 2B and 2C). The heavy chain peptide 35-71 spans HCDR2

(51,52,52A,53-57) and 94-106 spans the HCDR3 (92-100, 100A,B,C,D,E,F,G,H,I,J,K,101-102) and light chain peptide 19-32 spans LCDR1 (27, 27A,B,C, 28-32), 38-74 spans LCDR2 (49-52) and 87-103 spans LCDR3 (89-95,95A,96-98). Importantly, we also observed peptides spanning residues 243-269 (*ij* hairpin) from the E-protein intradimer interface in ZIKV showing decreased exchange upon C10 binding suggesting Fab C10 binding stabilized the entire ZIKV particle (Figures 2B and 2C).

Decreased deuterium exchange upon Fab C10 binding to recombinant DENV2 sE protein

We next investigated Fab C10 interactions with recombinant DENV2 sE protein by HDXMS. Fab binding resulted in decreased deuterium exchange at multiple peptides corresponding to the epitope on E-protein (58-73, 83-107, 313-322 and 352-367) as well as peptides (238-260, 270-278) (Figures S2D and S2E). Corresponding decreases in deuterium exchange in the Fab paratope were observed at peptides spanning the heavy (50-76) and light chains (50-74, 75-81)) (Figure S2F-4H). Additionally, decreased exchange at the intra-dimer interface residues in peptides spanning residues 238-260 indicated that Fab binding resulted in reduced intradimer dynamics in the recombinant sE-protein dimer.

Increased deuterium exchange across the DENV2 surface at saturating Fab concentrations.

164 To map interactions of Fab C10 binding with DENV2 virus particles, Fab C10:DENV2
165 complexation was carried out by saturating DENV2 with Fab C10 - molar ratio of approximately
166 3 Fab: 3 E protein. Under our experimental conditions, we identified 13 optimal pepsin fragment
167 peptides each for C10 heavy (sequence coverage ~82.5%) and light chains (sequence coverage
168 ~97.2%) (Figures S1C). 1, 36 and 5 peptides of proteins C (sequence coverage ~10%), E (sequence
169 coverage ~60.5%) and M (sequence coverage ~56%) were identified for DENV2 (Figures S1C).

170 In contrast to Fab C10:ZIKV HDXMS results, none of the peptides across DENV2 E and
171 M proteins showed any decreases in deuterium exchange, as might be expected at the Fab:DENV2
172 interface (Lim et al. 2017b). Instead, unexpectedly large increases in average deuterium exchange
173 were detected across multiple peptides from E (Figure 3A) and M proteins (Figure S4C) in the Fab
174 C10:DENV2 complex. A closer examination of the mass spectral envelope of the peptides showing
175 increased average deuterium exchange revealed a broadening of the isotope envelope width with
176 significantly more isotopic peaks in deuterium exchange peptides from E and M-proteins when
177 comparing Fab bound and unbound DENV2 viral particles (Figure 3G). Mass spectra for
178 deuterium exchange in representative peptides spanning epitope sites- peptides 78-103, 83-107 (*c*
179 strand, *cd* loop), 214-230 (*hh'* hairpin), 238-260 (*ij* hairpin) and 352-377 (DE loop) are shown in
180 Figure 3G. The extent of peak broadening was not equivalent for all peptides. Certain peptides
181 such as residues 31-42 (C_0 strand, C_0D_0 loop and D_0 strand) showed no peak broadening. The

broadening of peak width is reflective of the presence of multiple protein/particle conformations (Weis et al., 2006). These included peptides spanning the E protein N-terminus (residues 1-10), glycosylation sites (residues 57-69 (*a* and *b* strands) and 152-163) (E_0F_0 loop), E-interdimer interface ((residues 78-107) (*c* strand, *cd* loop) and residues 214-230 (*hh'* hairpin)) and E-intradimer interface (238-260 (*ij* hairpin) and 270-278 (*kl* hairpin)) (Figures 3A and 3B). Several of these peptides (Table S1) spanned the epitope residues previously identified (Rouvinski et al., 2015). In addition, we also detected increases in deuterium exchange in peptides spanning the stem helix (residues 27-47) of M-protein (Figure S4C).

The broader spread of the spectral envelopes shows low and high exchanging populations indicating that Fab C10 when bound to DENV2 increased the number DENV2 conformations. The high exchanging population, represents the regions with more rapid kinetics of association/re-association of Fab C10 to E-protein on the DENV2 viral surface. Notably, loci exhibiting increased deuterium exchange localized to E-protein dimer interface contacts in Fab C10:DENV2 (peptides 214-230 (*hh'* hairpin at the interdimer interface) and 238-260 (*ij* hairpin) (intradimer interface) indicating propagated increases in dynamics across the Fab C10:bound DENV2 viral particle. The above two dimer interface peptides are outside the epitope residues identified by X-ray crystallography (Table S1) (Rouvinski et al., 2015).

Fab paratope peptides showed characteristic decreases in exchange. These included the heavy (residues 50-76 (spanning HCDR2) and 104-112 (spanning HCDR3)) and light (residues 17-44 (spanning LCDR1), 50-74 (spanning LCDR2) and 80-106 (spanning LCDR3) chain peptides (Figures 3C, 3D and 3E). Overall, Fab C10 binding resulted in increased exchange in DENV2 E protein, mapped on the virus particle (marked red in Figures 3B, G) and decreased exchange in specific heavy and light chain peptides from Fab C10 (marked blue in Figure 3E). Furthermore, comparable decreases in exchange across paratope sites in Fab C10 were seen in both Fab C10:DENV2 and Fab C10-recombinant sE protein complexes. This indicated that Fab C10 is tightly bound to DENV2 without impacting the association/dissociation kinetics.

Fab C10 at Fab:E molar ratio of 3:3 induce large scale changes in DENV2

We next tracked Fab C10 interactions with DENV2 at sub-stoichiometric molar ratios of 1Fab:3E and 2Fab:3E by HDXMS. Decreases in deuterium exchange in E protein peptides spanning the C10 epitopes were detected at these molar ratios. Specifically, the 1Fab:3E molar ratio sample, we detected decreases in deuterium exchange in peptides spanning C10 epitopes (residues 78-107, 307-321, 322-338 and 352-377) (Figures 4A and 4B). Importantly, peptide 78-107 also mediates interdimer interactions on DENV2. Interestingly, the effects of Fab C10 binding

at inducing increased dynamics at sub-stoichiometric Fab concentrations were also observed at the two glycosylation sites (peptides 57-69 and 152-163) (Figures 4A and 4B). For easier comparison, deuterium exchange difference plots of sub-stoichiometric and saturating concentrations of Fab C10:DENV2 are shown side-by-side in Figure S3A-C. This indicated that Fab C10 binding greatly increased the dynamics of the glycan loops on DENV2. Importantly, long-range propagated conformational changes arising from Fab C10 binding to E-monomers were also detected as increases in deuterium exchange observed in peptides spanning the stem helices (residues 27-47) of M protein (Figure S4C). At the molar ratio of 2Fab:3E, similar magnitude decreases in deuterium exchange were observed in peptides spanning the C10 epitope (residues 78-107, 307-321, 322-338 and 352-377) (Figures 4C, and 4D). Increases in deuterium exchange were now seen in peptides spanning the E-intradimer interface (residues 238-260) (Figures 4C and 4D) reflecting an induced conformational distortion at the E-intradimer interface. A closer examination of the isotopic envelopes of peptides spanning the C10 recognition site on the E protein, revealed a characteristic bimodal envelope that was specific to the ratio of Fab C10 to DENV2 E protein and reflected the mixture of Fab C10-bound and unbound E protein present at sub-stoichiometric ratios. With increasing Fab C10 concentration, this envelope shifted to the right to merge into a higher exchanging population expanding the overall width of the isotopic envelope (Figure 4E).

233 An ensemble behavior of DENV2 E and M proteins in solution can be gleaned from deconvolution
234 of mass spectral envelopes (Figure S4).

235 Importantly, Fab C10 binding elicited long-range conformational changes across the entire
236 DENV2 virion (Figures 4F and 4G). A close-up of the spectral envelope showed that Fab C10
237 binding elicited increased exchange of the higher exchanging species. Centroids (filled triangles
238 (Figure 4E)) of the higher exchanging species (green dashed lines) for substoichiometric Fab
239 C10:DENV2 complexes were shifted to the right compared to uncomplexed DENV2. Incremental
240 induced allosteric effects of Fab C10 binding (interdimer and inter-raft interaction peptides 214-
241 230 (*hh'* hairpin), intra-dimer 238-260 (*ij* hairpin)) resulted in an increase in the weighted average
242 deuterium exchange. The greatest magnitude average increases in deuterium exchange were seen
243 in fully saturated Fab C10:DENV2 complexes (Figure 4H). To measure the conformational
244 heterogeneity induced by increasing Fab C10 binding, we applied a deconvolution function on
245 mass spectral envelopes of deuterium exchanged peptides showing spectral broadening using a
246 deuterium exchange mass spectral analysis program, HDExaminer version 3.2 (Sierra Analytics,
247 Modesto CA). Certain peptides, at substoichiometric concentrations of Fab C10, generated
248 bimodal mass spectra of deuterium exchanged states that could be deconvolved into two isotopic
249 envelopes, each representing a separate deuterium exchanging conformation within the ensemble.
250 The results of this deconvolution are shown in Figure S4 for peptides 83-107, 238-260 and 33-47

from the M-protein. Not all peptides showed bimodal distributions, E (4-10, 31-42, 199-205, 202-213, 214-230 and 378-387) showed unimodal exchange in all states examined. It should be noted that the deconvolution function used here broadly approximates mass spectral broadening into two conformational subpopulations which does not preclude the presence of additional minor conformational subpopulations. However, it offers insights into ensemble behavior upon C10 binding by identifying loci showing conformational heterogeneity across the E-protein.

Expectedly, similar decreases in deuterium exchange were observed in peptides spanning the Fab heavy and light chain in Fab C10:DENV2 complexes at both sub-stoichiometric Fab:E ratios (Figures S3D, S3E and S3F). Additionally, decreases in deuterium exchange were observed in peptides spanning Fab paratope heavy (residues 50-76) and light (residues 50-74, 75-81) chains at saturating 3Fab:3E molar ratios (Figures 3C and 3D).

These results suggest that Fabs at all stoichiometric ratios were bound tightly to the E protein on the viral surface, while the overall dynamics of the E protein across the virus increased drastically at saturating Fab C10 concentrations (3Fab:3E) (Figure S3C, Figure S4).

CryoEM structures of Fab C10:DENV2 at different Fab C10:E molar ratios reveal preferential Fab C10 binding to L2 E dimers on DENV2 surface

We mixed Fabs with DENV2 at different Fab:E molar ratios of 1:3, 2:3 and 3:3 at 28^{o}C before flash freezing on cryoEM grids. After imaging, during the cryoEM image reconstruction process, we conducted 2D and 3D classifications of picked particles from the cryoEM micrograph, and then averaged the particles within their respective class. We observed increased distorted/elliptical particles with increasing Fab concentration. At Fab:E molar ratios of 1:3, 2:3 and 3:3, we observed 0%, 3% and 60.4% distorted particles, respectively (Figure. 5A, 5B and 5C). This suggests increased Fab binding can cause the distortion of viral particles. However, we are unable to determine the structure of these distorted particles, due to heterogeneity of the particles and also the inherent high dynamics/structural disorder.

We have determined the cryoEM structures of the intact spherical Fab C10:DENV2 complex particles at 1Fab:3E, 2Fab:3E, 3Fab:3E molar ratios, to 3.1 Å, 3.3 Å and 3.6 Å, respectively (Figures 6A and 6B, 6C, S6 and Table S3). The 1Fab:3E and 2Fab:3E cryoEM maps showed no binding to I2 dimer and gradual increase in binding to the L2 dimer (A-C dimer) with increasing Fab concentrations. Only at 3Fab:3E molar ratio, weak Fab densities were observed on the I2 dimer, while those on the L2 dimers were much stronger (Figures 6A and 6C). We calculated the Fabs occupancies on the three individual epitopes in an asymmetric unit for all molar ratios of Fab:E protein cryoEM maps (Figure 6D). The maximum Fab occupancy is always on the epitope

on L2 dimer, but it only reaches a maximum of 59% even at saturated Fab concentrations. This suggests that all the epitopes are not equally optimal for Fab binding.

To map interactions of Fab C10 with DENV2, we used the cryoEM map of the Fab C10:DENV2 complex at 3:3 Fab:E molar ratio, determined to an overall resolution of 3.6 Å. However, the local resolution of the Fab and the E proteins interacting interface is 4.5 Å (Figure 6G, S5A) and therefore we could only deduce their interacting residues by using 8 Å distance cutoffs between Cα chains. The C10 epitope straddles across the E protein protomers within the dimer at the intradimer interface. Most of the residues in the epitope are the same between the L2 and I2 dimers (Figure 6E). Part of the epitope is on an E-protein protomer - the *b* strand (residues 67-73), the *bc* loop (residues 69-82), the fusion loop (residues 102-106) and the ij hairpin (residues 246-247). The other part of the epitope is on the other E-protein protomer - the D_0 strand (residues 46-47 on DI), the D_0-a loop (residues 52 and 54 on DII), the glycan loop (residues 148,149,153 and 155-156 on DII), the *kl* hairpin (residues 273-274 on DII) and the DIII ABE β-sheet region (residues 309,325 and 361-364) (Figure 6E and 6G).

There are also differences in the C10 epitopes on the L2 and I2 dimers, due to differences in their local environment. For the epitope on the I2 dimer, we observed that Fab C10 additionally binds residues across the inter-dimer E protein interfaces (Figure 6F). For the epitopes on both

ends of L2 dimer, one is located around the 5-f and the other, the 3-f vertices. The epitope around the 5-f vertex, in addition to the residues within the dimer, also consists of eight residues from a neighboring E protein across the inter-raft interface. They are mainly mediated by electrostatic interactions. On the other hand, the opposite epitope on the same L2 dimer around the 3-f vertex consists of residues identical to those on the I2 dimer. Therefore, the epitope around 5-f is unique compared to the other epitopes. In particular, the E protein rafts may display less tight contacts around the 5-f, facilitating C10 binding at higher temperatures. Notably, the interdimer and inter-raft residues are not critical for binding, as the Fab can also bind to soluble E dimer proteins, which do not have these higher quaternary E protein arrangements as those observed on the viral surface (Sharma et al., 2021).

CryoEM structure of DENV2 complexed with bivalent antibody

To investigate the binding of bivalent antibody, we used bivalent C10 F(ab')2 to complex with virus particles. When mixed in solution, massive aggregation was observed by cryoEM, preventing structural studies. To overcome this, we coated the C10 $F(ab')_2$, onto thin carbon and then added DENV2 particles, such that they were spaced out to reduce aggregation. We then added more $F(ab')_2$ to coat the virus surface. Our cryoEM images show some particles clustering together, but there are some individual particles that can be used for cryoEM reconstruction (Figure

7A). The final resolution of the resulting DENV2:F(ab')$_2$ map is 3.5 Å, and the antibody occupancy is low (Table S2), as it can only be visualized at low contour levels (Figure 7B). We conducted localized reconstruction of the E protein raft with C1 symmetry. Classification showed that class I forming 15 % of the masked raft, had one F(ab')$_2$ bivalently bound to two L2 E dimers, each around the 3-f vertex (Figure 7C). Class II (54% of the masked raft) had very low F(ab')$_2$ densities that were distributed evenly around the 5-, 3-, and 2-fold vertices. Class III, forming 29% of the masked raft, had no F(ab')$_2$ bound (Figure S7A). Comparison between the cryoEM maps of the class I DENV:F(ab')$_2$ localized reconstruction and the icosahedrally averaged whole DENV:Fab complexes (Figure S7B), showed that the distance between residues (Cys231) at the tip of the two Fab constant regions binding to the two neighboring 3-f vertices, is closer in the DENV: F(ab')$_2$ than the DENV:Fab map – ~40 Å versus ~100 Å (Figure S7C). This suggests that the two Fabs at neighboring 3-f vertices in the DENV: F(ab')$_2$ cryoEM map are derived from the same F(ab')$_2$.

Discussion

Bivalent antibody binding and neutralization mechanism

For cryoEM reconstruction of the DENV2: F(ab')$_2$ complex, we selected individual particles that did not aggregate, these particles may show more bivalent binding of a single F(ab')$_2$ to two

neighboring E protein dimers each around the 3-f vertices (Figure 7D). In this cryoEM map, the densities of Fabs of F(ab')$_2$ on the epitopes around the 5-fold or 2-fold vertices are very weak. However, we were still able to fit Fabs into the densities (Figure S7C). The angle and orientation of the two Fab molecules suggests they are not derived from a single F(ab')$_2$. Hence when a Fab arm of an IgG bound to one of these epitopes, the other Fab arm will not be able to engage any epitope within the same viral particle and hence this Fab arm will likely bind to other viral particles causing aggregation (Figure S7D). From the accompanying manuscript (Sharma et al., 2021), bivalency of IgG is important for neutralization for DENV2. There could be different neutralization mechanisms at different IgG concentrations. For example, it is possible at low antibody concentrations, because of the higher avidity of the IgG towards the two epitopes (each from a L2 dimer) around neighboring 3-f vertices, this could be the preferential way of antibody binding. At high antibody concentrations similar to that in our cryoEM studies with the F(ab')$_2$, the ability of F(ab')$_2$ to aggregate virus particles could become an important contributor of neutralization. We observed IgG, even at saturating concentrations, can only achieve partial occupancies. It is plausible that the bound IgG could cause vibrations/distortion to the surface inducing the unbound E protein to change into fusion conformation, thus leading to virus aggregation. Alternatively, it could just be a function of the bivalent antibody binding to different viral particles.

There are possibly many ways DENV could attach to different receptors on different cells e.g., DC-SIGN, heparin sulphate etc. In our attachment assay, we used BHK-21 cells and IgG C10 can partially block virus attachment to these cells. It was previously suggested that DIII and the glycosylation site on the E protein are important for virus attachment to host cell receptors (Hung et al., 2004). Since C10 epitope consists of these two sites, antibody binding may thus block virus interaction with some receptors. It may not be possible for an antibody to block all types of receptor binding, as there could be many receptors on different cell lines.

Regardless of which receptor the DENV engages, the virus will subsequently need to fuse with the endosomal membrane so that its viral genome can be released into the cell cytoplasm. Here we showed that Fab C10 can block structural changes that are required for fusion. It was previously known that fusion of virus to endosomal membrane is initiated by the structural re-organization of E proteins on the virus surface upon exposure to low pH. This involves the E protein protomers within a dimer dissociating from each other and then re-organizing into trimeric structures (Bressanelli et al., 2004). Since Fab C10 binds across E proteins at the intra-dimer interface, it will lock E protein protomers in a dimeric structure, thus preventing structural reorganization required for fusion.

During cryoEM reconstruction of the saturating concentrations Fab complexed with DENV2, we observed 60% of the particles become distorted. This suggests that at high antibody concentrations, there is an added mechanism of neutralization – by distortion of DENV particle.

Fab C10 binding induced contrasting effects on DENV2 and ZIKV

Our HDXMS results indicated that Fab C10 interacts with ZIKV resulting in overall decreased dynamics of the virus surface (Figure 2), whereas to DENV2, Fab induced an overall increase in dynamics (Figure 4H). However, the HDXMS of the Fab C10 paratope showing decreased dynamics suggesting the Fab is constantly tightly bound to its epitope. This is unexpected, as one would think that the highly mobile DENV2 surface will negatively impact Fab binding. Superposition of the residues comprising of the E protein epitopes (identified by cryoEM) and the peptides with increased dynamics detected by HDXMS shows only part of them are overlapping. Because HDXMS reports a combination of Fab binding and dynamics effects and is unable to distinguish whether the sites that are undergoing dynamics are bound or not bound by Fabs, a mixture of conformational states likely contribute to the read out as a composite average deuterium exchange signal.

In the accompanying paper (Sharma et al., 2021), their crystal structure of variable domain fragment (ScFv) of C10 complexed with DENV2 recombinant E protein, showed binding of scFv

C10 can induce hinge-like motions in the E protein dimer. We speculate that increasing Fab C10 beyond a threshold molar ratio of 2Fab:3E protein on the DENV2 surface, promotes a new ensemble, where a single Fab C10 binding to one site on a dimer, resulting in an overall re-arrangement of the dimer such that a second Fab C10 likely cannot bind at the second site on the same dimer (Sharma et al., 2021). Further, Fab C10 shows preferential binding to the L2 dimer. It is possible that binding to the less favorable I2 dimer, can be initiated only beyond the threshold molar ratio of 2Fab:3E protein, also induced further motions of the E proteins. This accounts for the higher overall deuterium exchange at saturating Fab C10 concentrations. These are also consistent with cryoEM results showing particle heterogeneity in the presence of saturating Fab C10.

Fab C10 prefers binding to L2 dimer than I2 dimer on the DENV2 surface

All our cryo EM maps showed the Fab densities on the I2 dimer are much weaker than at the L2 dimer. A possible reason why the Fab binds better to L2 than I2 dimer, is shown in the accompanying paper (Sharma et al., 2021) -- when the Fab C10 bind to part of its epitope ij loop, this will cause slight conformational changes to the connecting hh' hairpin. This hairpin motion can likely be accommodated better in the inter-raft region than the inter-dimer interface hence, allowing more Fabs to bind to L2 dimer. However, this slight changes in the hh' hairpin cannot be

observed in our cryoEM map due to the limitation of the resolution. Another reason could be the Fab also binds to additional E proteins across the inter-raft region when bound to L2 dimer compared to I2 dimer (Figure 6F).

Increase in Fab occupancy induces conformational changes and alters the dynamics of the surface E proteins in DENV2 particles

Given the high dynamics of E proteins detected by the HDXMS, it is surprising that we could obtain a high resolution cryoEM map of the Fab:DENV complex at the molar ratio of 3Fab:3E. Analysis of the local resolution (Figure S5A) and B-factor distribution (Figure S5B) suggests no large differences in mobility between the L2 and I2 dimers. Therefore it suggests that the cryoEM reconstructable spherical Fab:DENV2 particles are not that ones that are undergoing increased dynamics.

The Fab occupancies on the cryoEM reconstructable DENV2 spherical particles reach a maximum of only 59% at best at even saturating Fab concentration (molar ratio of 3Fab:3E) (Figure. 6D), suggesting that none of these epitopes on this spherical viral surface are the most optimal for Fab binding (Figure. 6A). The accompanying paper (Sharma et al., 2021) showed that Fab C10 when bound to DENV2 sE protein dimer, distorted the dimeric structure, perhaps this is

421 the most optimal conformation for Fab C10 binding. These conformational changes are restricted
422 in the context of the spherical viral particles, due to the extensive E-to-E interactions at the inter-
423 dimer and inter-raft interfaces and hence not observed in our cryoEM structure. However, from
424 the 2D and 3D class averages, we observed at saturating Fab concentrations, in total there are
425 60.4% distorted virus particles (which are not reconstructable), we speculate that on these particles,
426 there are higher Fab occupancies, this may push some E protein dimers to undergo conformational
427 changes, as observed in the crystal structure of Fab C10:sE protein in the accompanying paper.
428 This is consistent with the dramatic increase in dynamics detected by HDXMS for the 3Fab:3E
429 molar ratio compared to 1Fab:3E and 2Fab:3E (Figure S3A-C). Thus the increase in dynamics
430 detected by HDXMS, maybe contributed by these distorted particles which skew the weighted
431 average deuterium exchange across the sample.

432 The cryoEM structure of Fab C10-ZIKV complex showed mostly equal C10 densities on
433 their epitope across all asymmetric units under saturating C10 concentrations (Zhang et al., 2016).
434 This is consistent with the accompanying paper (Sharma et al., 2021). showing the paratope and
435 the ZIKV E protein dimer epitope complements each other very well and hence no distortion of E
436 protein is needed for optimal Fab binding. This is consistent with its strong Fab neutralization
437 activity for ZIKV (Sharma et al., 2021). Whereas for DENV2, because the optimal Fab binding

requires distortion of the E protein dimer on the virus surface, which is restricted due to virus quaternary structure, neutralizing activity of the Fab is hence much poorer (Sharma et al., 2021).

In conclusion, an antibody can neutralize virus through a combination of mechanisms: inhibition of attachment, inhibition of fusion, and inducing distortion of the virus surface. The ability of antibody to induce large-scale viral structural changes have not been widely studied, our current work shows the relationship of induced conformational changes by antibodies with the stability of virus quaternary structure.

Limitation of the Study

From our study, the dynamics induced by Fab occurs only upon binding to DENV2 and not ZIKV, that suggests antibody-induced distortion of virus particles is not part of the mechanism of neutralization for ZIKV. The ability of the antibody to partially block attachment and fusion (Zhang et al., 2016) and achieve full occupancy on the ZIKV surface are sufficient to cause neutralization. Based on the study by Sharma (Sharma et al., 2021), C10 has the similar binding and neutralization profile across DENV serotypes 2, 3 and 4. This suggests C10 most likely can also cause particle distortion to DENV3 and DENV4. However, this requires further evaluation by a combination of cryoEM and HDXMS.

The attachment assay used IgG antibodies while for HDXMS experiments, we could only analyze Fab complexes because IgG caused virus aggregation and sample heterogeneity thereby precluding HDXMS analysis. For cryoEM study on the IgG:DENV2 complex, we can only analyze the non-aggregated individual particles, even though the sample contain lots of aggregates. Therefore, HDXMS and cryoEM studies could only show limited information of the effect of IgG on virus particles.

STAR ★Methods

Key Resources Table

RESOURCE AVAILABILTY

Lead contact

Further information and requests for resources and reagents should be directed to and will be fulfilled by the lead contact, Ganesh Srinivasan Anand (gsa5089@psu.edu)

Materials Availability

This study did not generate new unique reagents

Data and code availability

- The cryoEM maps and coordinates have been deposited in the Protein Data Bank (PDB) and Electron Microscopy Data Bank (EDMB). DENV2:Fab C10 at Molar ratio of 1Fab:3E at 28 ℃: (EMDB: 31677, PDB: 7V3F), DENV2:Fab C10 at Molar ratio of 2Fab:3E at 28 ℃: (EMDB: 31678, PDB: 7V3G), DENV2:Fab C10 at Molar ratio of 3Fab:3E at 28 ℃: (EMDB: 31679, PDB: 7V3H), DENV2:F(ab')$_2$: (EMDB: 31682, whole map; EMDB: 31681, PDB: 7V3J, local map)
- This paper does not report original code
- Any additional information required to reanalyze the data reported in this paper is available from the lead contact upon request.

EXPERIMENTAL MODEL AND SUBJECT DETAILS

Purification of DENV2 (NGC) and ZIKV

Mature DENV2 (NGC) and ZIKV were produced and purified as below: Aedes albopictus C6/36 cells (ATCC) were grown in RPMI 1640 media supplemented with 2% fetal bovine serum at 29°C. At 80% confluency, the cells were inoculated with ZIKV H/PF/2013 strain at a multiplicity of infection (MOI) of 0.5 or DENV2 NGC strain at a MOI of 0.1 and incubated at 29°C for 4 days. The virus-containing media was clarified by centrifugation at 14,000 g for 1 h.

Virus was precipitated overnight from the supernatant using 8% (w/v) polyethylene glycol 8000 in NTE buffer (10 mM Tris-HCl pH 8.0, 120 mM NaCl and 1 mM EDTA) and the suspension was centrifuged at 14,000 g for 1 h. The resulting pellet containing the virus was resuspended in NTE buffer and then purified through a 24% (w/v) sucrose cushion followed by a linear 10%–30% w/v potassium tartrate gradient. The virus band, visualized by its light scattering ability, was extracted, buffer exchanged into NTE buffer and concentrated using a concentrator with 100-kDa molecular weight cut-off filter. All steps of the purification procedure were done at 4°C. Amounts and concentrations of purified DENV2 (NGC) and ZIVK particles were estimated by comparing the corresponding E-protein band intensity with the band intensities of BSA standards of known concentrations on as SDS PAGE gel stained with Coomassie Blue dye. Purified mature DENV2 (NGC) and ZIKV corresponding to 0.25 mg/mL and 0.1mg/mL of E-protein in the virus samples was used for subsequent HDXMS experiments.

Expression and purification of DENV2 recombinant E-protein

Drosophila melanogaster Schneider 2 cells (ThermoFisher (Invitrogen) Cat. No: R69007, Singapore) were transfected with pMT/BiP/V5-HisA plasmid encoding soluble deletion mutant of soluble E-protein (residues 1-394) from DENV2. Recombinant E-protein was glycosylated at identical positions (N67, N153) as viral E-protein as shown previously (Lim et al., 2017). Tissue

culture supernatant containing the recombinant E-protein was purified using 4.8 A affinity column, washed with 10 mM Tris-HCl and 150 mM NaCl, pH 5 and eluted with 0.1 M Glycine-HCl, pH 2.7. Eluted recombinant E-protein was dialyzed with 10 mM Tris-HCl, 150 mM NaCl, pH 7.5 and concentrated to a final concentration of 1.0 mg/mL.

Production of C10 Fab fragment

Soluble C10 IgG was expressed in HEK293T cells that were co-transfected with plasmids containing the C10 heavy and light chain variable regions sequences (Zhang et al., 2016) and purified by protein A affinity chromatography. Purified C10 IgG was subsequently resuspended in 200 mM HEPES, 100 mM NaCl, 50 mM NaOAc, pH 7.0. The Fab fragments of C10 were generated from overnight digestion of the purified IgG (8 mg/mL) with immobilized papain (Thermo scientific) at 37 °C. The Fab fragments were purified by anion exchange chromatography (resource Q, GE Healthcare) followed by gel filtration (Superdex 200 increase 10/300 GL, GE Healthcare) and subsequently concentrated to 3 mg/mL.

METHODS DETAILS

Formation of C10-ZIKV complex, C10-DENV2 complexes under differential C10 concentrations and C10-unassembled complexes

C10-ZIKV complex (C10-ZIKV)

Purified ZIKV was pre-equilibrated at 28 °C for 30 min followed by incubation of ZIKV with slight molar excess of C10 Fab fragment in a molar ratio of 1 E-protein : 1.2 Fab C10 to ensure saturated binding at 28 °C for 40 min.

C10- DENV2 complexes (C10-DENV2)

Purified unexpanded DENV2 (DENV2) was pre-equilibrated at 28 °C for 30 min followed by incubation of DENV2 with slight molar excess of C10 Fab fragment in a molar ratio of 1 E-protein: 1.2 Fab C10 to ensure saturated binding with Fab at 28 °C for 40 min.

DENV2 complexed with C10 fab fragments under non-saturated binding conditions (1:3 and 2:3 ratios of C10 to E-proteins)

Purified DENV2 was pre-equilibrated at 28 °C for 30 min followed by incubation of DENV2 with C10 Fab fragment in a molar ratio of 1 C10: 3 E-proteins or 2 C10: 3 E-proteins at 28 °C for 40 min.

C10-recombinant E-protein

Purified recombinant E-proteins (1.0 mg/mL) was equilibrated with the Fab fragment of C10 in a molar ratio of 1 unassembled E-protein: 1.2 Fab C10 for 40 min at 28 °C.

<u>CryoEM sample preparation</u>

Fab C10:DENV2 complex was formed as described above. The samples were incubated at 28 °C before freezing on cryoEM grids. The 400 mesh grids with a less than 3nm thick carbon lacey support (TED PELLA, INC) were glow-discharged at 5mA for 1min using Emitech K100X Glow Discharge Unit. About 2.1 µl of samples were applied to the grids, blotted with a filter paper (Ted Pella Standard Vitrobot filter paper, Grade 595) for 8s (Blot force 4, Blot Time 8 seconds, Drain time 0.5 seconds, Humidity 100%) to remove excess sample, and then flash frozen in liquid ethane by using the Vitrobot Mark IV plunger (FEI, Netherland). To ensure temperature consistency, the temperature of the Vitrobot humidity chamber was adjusted to 22 °C for blotting.

CryoEM image acquisition and reconstruction procedure

SerialEM was used to carry out the automated data collection. The data sets for 2Fab:3E molar ratio of 2:3 and F(ab')2 uses beam shift for acquisition. Image shift was used to target 6 exposures per stage position for Fab ratio 1:3 and 3:3 with an image shift of 1.6 um. Images for all samples were recorded by movie mode, with similar total exposure of 2.9 s, 25 frames per movie and total dose of 25 e-/Å2. The frames from each "movie" were aligned using MotionCor2 (Zheng et al., 2017) to produce full dose images used for particle selection and orientation search, and images from the first several frames amounting to the dose of about 18 e-/Å2 for use in 3D reconstruction.

554 The images were taken at underfocus in 0.8 to 2.0 μm range. In total, 3096, 2836, 3090 and 3819
555 micrographs were collected for Fab C10:DENV2 at Fab:E molar ratio of 1:3,2:3, 3:3 and the
556 F(ab')2:DENV2 complex, respectively. The astigmatic defocus parameters were estimated with
557 Patch CTF estimation in Cryosparc (Punjani et al., 2017) and is corrected during orientation search.
558 After automatically particle picking using Cryosparc, a total number of 355 475, 238 894, 235 059
559 and 120 326 particles of bin4 were selected for 20 rounds iterations of 2D classification in
560 Cryosparc to produce 2D class averages. The 20 rounds iterations of 3D reconstruction with C1
561 symmetry were done with CryoSparc and Relion (Scheres, 2012). The uncomplexed DENV2
562 (EMDB ID EMD-5520) was lowpass to 60 Å and used as the starting model. Classes with broken
563 and distorted particles were removed. 109 712, 70 534, 42 509 and 38 387 individual particles
564 from Fab C10:DENV2 at Fab:E molar ratio of 1:3,2:3, 3:3 and the F(ab')2:DENV2 complex,
565 respectively, were selected for further processing. Structure refinement was done, and icosahedral
566 symmetry were applied to improve the resolution. The 3D reconstruction procedure produced the
567 complex structures with resolutions of 3.1 Å, 3.3 Å, 3.6 Å and 3.6 Å for Fab C10:DENV2 at Fab:E
568 molar ratio of 1:3, 2:3, 3:3 and the F(ab')2:DENV2 complex using the Fourier shell correlation
569 cutoff of 0.143 (Figure S6, Table S3). Local map resolution was estimated with ResMap
570 (Kucukelbir et al., 2014).

571 To further investigate the structures of FabC10:DENV2 (molar ratio 3Fab:3E) and also the
572 F(ab')2:DENV2 around the 2-fold vertices, we used Relion symmetry expansion and Scipion (De
573 la Rosa-Trevín et al., 2016) to extract subregions and perform localized reconstruction described
574 as below (Ilca et al., 2015). After 3D refinement with imposition of icosahedral symmetry, we
575 extracted sub-particles from the 2-fold region or the asymmetry in a box-size of 220×220 pixels
576 and expanded the sub-particles with I4 symmetry. The extracted sub-particles were used to
577 generate the initial model using relion_reconstruct. 3D classification was then performed without
578 alignment. Further refinement of best class of the FabC10:E protein raft (molar ratio 3Fab:3E) map
579 led to a structure at 3.9 Å resolution, the class of $F(ab')_2$:E protein raft map, at 4.6 Å resolution.
580 The resolution was assessed by Fourier shell correlation curve with a cutoff at 0.143 from two
581 independent half-sets of the sub-particles. Local map resolution was estimated with ResMap
582 (Kucukelbir et al., 2014).

583 Protein structure building

584 The C10-DENV2 structures were interpreted by fitting in the free DENV2 (PDB ID 3J27) and Fab
585 C10 (PDB ID 4UT9) first as rigid bodies in Chimera (Pettersen et al., 2004) and then refined with
586 phenix.real_space_refine with default parameters plus rigid body refinement and secondary-
587 structure and torsion restraints (Afonine et al., 2018) and COOT was used to fix regions manually

588 with poor geometry. (Emsley and Cowtan, 2004). The refined subunits were used to build the
589 biological unit with the command sym in Chimera. The final coordinates of the asymmetric units
590 were checked by MolProbity. Maps and structures shown in the figures were generated with
591 PyMOL, Chimera and Coot.

592 Fab occupancy calculation

593 the Fab occupancies on the three individual epitopes within an asymmetric unit were calculated by
594 comparing the densities of the Fab with that of the E protein dimer in the "fit in map" tool in the
595 program "Chimera". The parameter "average map value" represent the trilinear interpolation of
596 map gray values from the eight corners of the data cell enclosing each atom position. The ratio of
597 the "average map values" for Fab to E protein was used to quantify Fab occupancy at each Fab
598 binding site. The formula is the average map value of $(Fab \div E\ dimer) \times 100\%$

599 5.2.4 Amide hydrogen/deuterium exchange of C10-ZIKV complex, C10-DENV2 complexes,
600 C10-recombinant E-proteins and Fab C10

601 Deuterium exchange buffer was prepared by solubilizing lyophilized NTE (12 mM Tris-
602 HCl, pH 8.0, 120 mM NaCl, 1 mM EDTA) buffer in 99.9% D_2O. D_2O NTE buffers were incubated
603 separately at 28 and 37 °C for 30 min prior to deuterium exchange reactions to ensure temperature
604 consistency during HDX labelling reactions. Amide hydrogen/deuterium exchange of C10-

DENV2 complexes were initiated by 10X dilution of C10-DENV2 complexes with temperature equilibrated D_2O NTE buffers (final D_2O concentration of 89.9%). HDX of Fab C10 (3 mg/mL) was carried with D_2O NTE buffer equilibrated at 37 °C and HDX of sE (1.0 mg/mL) and C10-sE complexes were carried out with D_2O NTE buffer equilibrated at 28 °C.

We selected a single deuterium exchange time point of 1 min as we have previously shown that the deuterium exchange times from 1 min to 60 min showed minimal differences in the extent of deuteration across all the peptide in DENV2 (Lim et al., 2017). Furthermore, at fast timescales, HDXMS reports on changes at the antibody-antigen interface and any associated propagated conformational fluctuations detectable at these experimental timescales (Mandell et al., 1998). Hence, the shortest time point of 1 min offered a suitable window for mapping interaction interfaces of C10 with ZIKV by HDXMS. As such, deuterium exchange of free ZIKV and C10-ZIKV complex were carried out for 1 min.

Deuterium exchange labelling for all reactions were carried out for 1 min and carefully maintained at their respective indicated temperatures of 28 °C and 37 °C. Deuterium exchange were quenched by lowering the pHread to 2.5 upon addition of cold NaOH in GnHCl and Tris(2-carboxyethyl) phosphine hydrochloride (TCEP-HCl) to a final concentration of 1.5M GnHCl and 0.25M TCEP-HCl. 0.1 mg of titanium dioxide (TiO_2) were added to the quenched reaction mixture

and incubated for 1 min with mixing at 30 s on ice to remove viral membrane phospholipids. TiO_2 were removed from the sample with 0.22 µm filter by centrifugation at 14,549g for 1 min at 4 °C. Collectively, TiO_2 treatment step resulted in an addition of 2 min to the sample handling time. In the case of recombinant E-proteins, C10-recombinant E-proteins and Fab C10, where viral phospholipids were not present, TiO_2 treatment step was replaced with 2 min incubation on ice to ensure equivalent post-quenching sample treatment time between C10-DENV2 complexes and these samples. All deuterium exchange reactions were performed in triplicate, and the reported values for every peptide are an average of three independent reactions without correcting for back exchange.

Pepsin digestion and liquid chromatography coupled to mass spectrometry

Quenched samples were injected into a chilled nano-UPLC HDX sample manager (Waters, Milford, MA) as described by Wales et al. (Wales and Engen, 2006) and subjected to online pepsin digestion using the Waters Enzymate BEH pepsin (2.1 X 30 mm) column in 0.05% formic acid in water at 100 ml min^{-1}. Pepsin proteolysis peptides from the samples were trapped using a 2.1 mm X 5 mm C18 trap column (ACQUITY BEH C18 VanGuard Pre-column, 1.7 mm, Waters, Milford, MA) and eluted using an 8–40% gradient of acetonitrile in 0.1% formic acid at 40 ml min^{-1} into a reverse phase column (ACQUITY UPLC BEH C18 Column, 1.0 X 100 mm, 1.7 mm, Waters) by

nanoACQUITY Binary Solvent Manager (Waters, Milford, MA). Peptides were ionized by electrospray into SYNAPT G2-Si mass spectrometer (Waters, Milford, MA) acquiring in $HDMS^E$ mode (Li et al., 2009) for detection and mass-measurements with ion mobility activated at wave height of 40V and velocity of 600 m/s. Peptides separated after ion mobility separation were carried by the transfer wave at height of 4V and velocity of 197m/s. 200 fmol/µl of [Glu^1]-fibrinopeptide B ([Glu^1]-Fib) was simultaneously injected into the mass spectrometer at a flow rate of 10 µL/min for continuous calibration during sample acquisition.

Mass spectrometric identification of peptides and determination of deuterium uptake

Peptides of C-, E- and M-proteins from ZIKV and DENV2 were identified through independent searches of mass spectra from the undeuterated samples against individual ZIKV and DENV2 database containing the amino acid sequences of all the three structural proteins using PROTEIN LYNX GLOBAL SERVER version 3.0 (Waters, Milford, MA) software. Mass spectra of peptides from a single undeuterated sample were filtered using precursor ion mass tolerance of < 10 ppm, and products per amino acids of at least 0.2 with a minimum intensity of 5000 for both precursor and product ions. Five and three undeuterated samples were collected for DENV2 (NGC) and ZIKV samples respectively, and the final peptide list includes only peptides that fulfilled the above described criteria and were identified independently in at least 3 of the 5

undeuterated samples. In DENV2 dataset, the three glycopeptides (57-68, 57-69, 152-163) we similarly identified in DENV2 E-protein with the glycans detected in several of the fragment peptides as indicated from the previous study (Lim et al., 2017). Peptides of C-, E- and M protein from C10-DENV2 and ZIKV complexes were independently identified by searching the mass spectra of the undeuterated samples of the C10-DENV2 or C10-ZIKV complexes against their respective peptide list and were selected if they were identified independently in a minimum of 2 out of 3 undeuterated samples.

Peptides from recombinant E-protein were identified by searching the mass spectra of the undeuterated sample against a database containing the amino acid sequence of DENV2 (NGC) E-protein (1-394) and filtered according to the search criteria as indicated above. Mass spectra from three undeuterated samples were collected and peptides were retained if they were independently identified in a minimum of two out of three undeuterated samples. Peptides of the heavy and light chain of Fab C10 were identified by searching the mass spectra of the undeuterated sample against a database containing the heavy and light chain amino acid sequences following the search criteria as described above. Selected peptides were independently identified in at least 2 out of the three undeuterated samples. Corresponding heavy and light chain peptides of C10 from the C10-DENV2 complexes and C10-recombinant E-proteins were searched against this peptide list and selected if they were independently identified in at least 2 of the 3 undeuterated samples.

674 Deuterium uptake and determination of deuterium exchange differences

675 Deuterium uptake in all peptides were determined by subtracting the average mass centroid
676 of deuterium exchanged peptides with the respective undeuterated peptides as described in the
677 previous chapters. The difference in absolute number of deuterons between the two states
678 compared was calculated by subtracting centroid masses of deuterated peptides between two
679 experimental conditions. The differences in deuterons exchanged for all peptides from C-, E- and
680 M-protein from DENV2/ZIKV and the heavy and light chain of C10 are represented in individual
681 difference plots. The standard deviations for deuterium uptake in all peptides were determined and
682 a difference of 0.5 Da was used as the significance threshold for differences in deuterium uptake
683 across the two states compared and agrees with the observed standard errors measured in
684 deuterated peptides (Houde et al., 2011).

685

686 Deconvolution analysis of deuterium exchange mass spectral envelopes

687 Deconvolution of mass spectral envelopes was carried out by HDExaminer version 3.2
688 (Sierra Analytics, Modesto CA) to check for ensemble behavior in solution, specifically to check
689 for two distinct distributions of mass spectral envelopes. Each of these envelopes would
690 represent distinct conformations in solution (Weis et al., 2006). We set a threshold fit value

score of 0.9 for the goodness of fit of the experimental mass spectral envelope for deuterium exchanged peptides with the theoretical envelope. If the fit score for a peptide is less than the threshold, the program will fit the spectral envelope to a bimodal distribution. If the score of the bimodal distribution is greater than that of the unimodal distribution, the program assigns a lower exchanging (left population) and a higher exchanging (right population). Results from deconvolution for three representative mass spectra are shown in Figure S4.

Quantification and Statistical Analysis

Statistical analysis

Where appropriate, statistical details are provided in the STAR Methods and figure legends.

Acknowledgments

We thank Victor Kostyuchenko and Guntur Fibriansah for technical support. This work was supported by NRF (NRF2017NRF-CRP001-027) and MOE Tier 3 grant (MOE2012-T3-1-008) awarded to G.A. and S.M.L., Startup funding from The Pennsylvania State University to G.A., National Research Foundation Investigatorship award (NRF-NRFI2016-01) and National Research Foundation competitive Research Project grant (NRF2016NRF-CRP001-063) awarded and the Duke-NUS Signature Research Programme funded by the Ministry of Health, Singapore awarded to S.M.L. We thank Felix Rey for $F(ab')_2$ antibody

and discussions. We also thank Theresa Buckley, Sean Braet and Varun Venkatakrishnan, Department of Chem for helpful discussions.

Author Contribution

G.A. and S.M.L. co-supervised the project. G.S. provided antibodies. G.A. and X.X.L. did the hydrogen-deuterium exchange mass spectrometry analysis. B.S. and S.J.Z. did the cryo-EM image reconstruction. S.M.L., B.S. and S.J.Z. interpreted the cryo-EM maps and conducted the structural analysis. B.S., X.N.L. and S.V.C. purified the virus for cryo-EM and HDXMS studies. T.S.N., A.T.W.K. and J.S. collected cryo-EM data. G.A., S.M.L., X.X.L., S.J.Z. and B.S. analyzed the data and wrote the manuscript.

DECLARATION OF INTERESTS

The authors declare no competing interests.

References

1. Afonine, P.V., Poon, B.K., Read, R.J., Sobolev, O.V., Terwilliger, T.C., Urzhumtsev, A., and Adams, P.D. (2018). Real-space refinement in PHENIX for cryo-EM and crystallography. Acta Crystallogr D Struct Biol *74*, 531-544.
2. Barba-Spaeth, G., Dejnirattisai, W., Rouvinski, A., Vaney, M.C., Medits, I., Sharma, A., Simon-Loriere, E., Sakuntabhai, A., Cao-Lormeau, V.M., Haouz, A.*, et al.* (2016). Structural basis of potent Zika-dengue virus antibody cross-neutralization. Nature *536*, 48-53.

3. Bhatt, S., Gething, P.W., Brady, O.J., Messina, J.P., Farlow, A.W., Moyes, C.L., Drake, J.M., Brownstein, J.S., Hoen, A.G., Sankoh, O.*, et al.* (2013). The global distribution and burden of dengue. Nature *496*, 504-507.
4. Bressanelli, S., Stiasny, K., Allison, S.L., Stura, E.A., Duquerroy, S., Lescar, J., Heinz, F.X., and Rey, F.A. (2004). Structure of a flavivirus envelope glycoprotein in its low-pH-induced membrane fusion conformation. EMBO J 23, 728-738.
5. de la Rosa-Trevin, J.M., Quintana, A., Del Cano, L., Zaldivar, A., Foche, I., Gutierrez, J., Gomez-Blanco, J., Burguet-Castell, J., Cuenca-Alba, J., Abrishami, V.*, et al.* (2016). Scipion: A software framework toward integration, reproducibility and validation in 3D electron microscopy. J Struct Biol *195*, 93-99.
6. Dejnirattisai, W., Wongwiwat, W., Supasa, S., Zhang, X., Dai, X., Rouvinski, A., Jumnainsong, A., Edwards, C., Quyen, N.T., Duangchinda, T.*, et al.* (2015). A new class of highly potent, broadly neutralizing antibodies isolated from viremic patients infected with dengue virus. Nat Immunol *16*, 170-177.
7. Emsley, P., and Cowtan, K. (2004). Coot: model-building tools for molecular graphics. Acta Crystallogr D Biol Crystallogr *60*, 2126-2132.
8. Englander, S.W., and Kallenbach, N.R. (1983). Hydrogen exchange and structural dynamics of proteins and nucleic acids. Q Rev Biophys *16*, 521-655.
9. Fibriansah, G., Ng, T.S., Kostyuchenko, V.A., Lee, J., Lee, S., Wang, J.Q., and Lok, S.M. (2013). Structural Changes in Dengue Virus When Exposed to a Temperature of 37 degrees C. J Virol *87*, 7585-7592.
10. Houde, D., Berkowitz, S.A., and Engen, J.R. (2011). The utility of hydrogen/deuterium exchange mass spectrometry in biopharmaceutical comparability studies. J Pharm Sci *100*, 2071-2086.
11. Hung, J.J., Hsieh, M.T., Young, M.J., Kao, C.L., King, C.C., and Chang, W. (2004). An external loop region of domain III of dengue virus type 2 envelope protein is involved in serotype-specific binding to mosquito but not mammalian cells. J Virol 78, 378-388.
12. Ilca, S.L., Kotecha, A., Sun, X., Poranen, M.M., Stuart, D.I., and Huiskonen, J.T. (2015). Localized reconstruction of subunits from electron cryomicroscopy images of macromolecular complexes. Nat Commun *6*, 8843.
13. Kostyuchenko, V.A., Lim, E.X., Zhang, S., Fibriansah, G., Ng, T.S., Ooi, J.S., Shi, J., and Lok, S.M. (2016). Structure of the thermally stable Zika virus. Nature *533*, 425-428.
14. Kucukelbir, A., Sigworth, F.J., and Tagare, H.D. (2014). Quantifying the local resolution of cryo-EM density maps. Nat Methods *11*, 63-65.
15. Kuhn, R.J., Dowd, K.A., Beth Post, C., and Pierson, T.C. (2015). Shake, rattle, and roll: Impact of the dynamics of flavivirus particles on their interactions with the host. Virology *479-480*, 508-517.

16. Kuhn, R.J., Zhang, W., Rossmann, M.G., Pletnev, S.V., Corver, J., Lenches, E., Jones, C.T., Mukhopadhyay, S., Chipman, P.R., Strauss, E.G*., et al.* (2002). Structure of dengue virus: implications for flavivirus organization, maturation, and fusion. Cell *108*, 717-725.
17. Li, G.Z., Vissers, J.P., Silva, J.C., Golick, D., Gorenstein, M.V., and Geromanos, S.J. (2009). Database searching and accounting of multiplexed precursor and product ion spectra from the data independent analysis of simple and complex peptide mixtures. Proteomics *9*, 1696-1719.
18. Lim, X.X., Chandramohan, A., Lim, X.E., Crowe, J.E., Jr., Lok, S.M., and Anand, G.S. (2017a). Epitope and Paratope Mapping Reveals Temperature-Dependent Alterations in the Dengue-Antibody Interface. Structure *25*, 1391-1402 e1393.
19. Lim, X.X., Chandramohan, A., Lim, X.Y., Bag, N., Sharma, K.K., Wirawan, M., Wohland, T., Lok, S.M., and Anand, G.S. (2017b). Conformational changes in intact dengue virus reveal serotype-specific expansion. Nat Commun *8*, 14339.
20. Mandell, J.G., Falick, A.M., and Komives, E.A. (1998). Identification of protein-protein interfaces by decreased amide proton solvent accessibility. Proc Natl Acad Sci U S A *95*, 14705-14710.
21. Modis, Y., Ogata, S., Clements, D., and Harrison, S.C. (2003). A ligand-binding pocket in the dengue virus envelope glycoprotein. P Natl Acad Sci USA *100*, 6986-6991.
22. Pettersen, E.F., Goddard, T.D., Huang, C.C., Couch, G.S., Greenblatt, D.M., Meng, E.C., and Ferrin, T.E. (2004). UCSF Chimera--a visualization system for exploratory research and analysis. J Comput Chem *25*, 1605-1612.
23. Punjani, A., Rubinstein, J.L., Fleet, D.J., Brubaker, M.A. (2017). cryoSPARC: Algorithms for rapid unsupervised cryo-EM structure determination. Nat Methods 14, 290–296.
24. Rouvinski, A., Guardado-Calvo, P., Barba-Spaeth, G., Duquerroy, S., Vaney, M.C., Kikuti, C.M., Navarro Sanchez, M.E., Dejnirattisai, W., Wongwiwat, W., Haouz, A*., et al.* (2015). Recognition determinants of broadly neutralizing human antibodies against dengue viruses. Nature *520*, 109-113.
25. Scheres, S.H. (2012). RELION: implementation of a Bayesian approach to cryo-EM structure determination. J Struct Biol *180*, 519-530.
26. Wales, T.E., and Engen, J.R. (2006). Hydrogen exchange mass spectrometry for the analysis of protein dynamics. Mass Spectrom Rev *25*, 158-170.
27. Weis, D.D., Wales, T.E., Engen, J.R., Hotchko, M., and Ten Eyck, L.F. (2006). Identification and characterization of EX1 kinetics in H/D exchange mass spectrometry by peak width analysis. J Am Soc Mass Spectrom *17*, 1498-1509.
28. Westaway, E.G., Brinton, M.A., Gaidamovich, S., Horzinek, M.C., Igarashi, A., Kaariainen, L., Lvov, D.K., Porterfield, J.S., Russell, P.K., and Trent, D.W. (1985). Flaviviridae. Intervirology *24*, 183-192.

29. Whitehead, S.S., Blaney, J.E., Durbin, A.P., and Murphy, B.R. (2007). Prospects for a dengue virus vaccine. Nat Rev Microbiol *5*, 518-528.
30. Xie, H., Chakraborty, A., Ahn, J., Yu, Y.Q., Dakshinamoorthy, D.P., Gilar, M., Chen, W., Skilton, S.J., and Mazzeo, J.R. (2010). Rapid comparison of a candidate biosimilar to an innovator monoclonal antibody with advanced liquid chromatography and mass spectrometry technologies. MAbs *2*, 379-394.
31. Zhang, S., Kostyuchenko, V.A., Ng, T.S., Lim, X.N., Ooi, J.S., Lambert, S., Tan, T.Y., Widman, D.G., Shi, J., Baric, R.S*., et al.* (2016). Neutralization mechanism of a highly potent antibody against Zika virus. Nat Commun *7*, 13679.
32. Zhang, X.K., Ge, P., Yu, X.K., Brannan, J.M., Bi, G.Q., Zhang, Q.F., Schein, S., and Zhou, Z.H. (2013a). Cryo-EM structure of the mature dengue virus at 3.5-angstrom resolution. Nat Struct Mol Biol *20*, 105-U133.
33. Zhang, X., Sheng, J., Plevka, P., Kuhn, R.J., Diamond, M.S., and Rossmann, M.G. (2013b). Dengue structure differs at the temperatures of its human and mosquito hosts. Proc Natl Acad Sci U S A *110*, 6795-6799.
34. Zheng, S.Q., Palovcak, E., Armache, J.P., Verba, K.A., Cheng, Y., and Agard, D.A. (2017). MotionCor2: anisotropic correction of beam-induced motion for improved cryo-electron microscopy. Nat Methods *14*, 331-332.

Figure Legends:

Figure 1: the neutralization of antibody C10. A) RT-qPCR attachment assays shows C10 IgG when complexed with either DENV2 or ZIKV particles can partially inhibit them from attaching BHK-21 cells. Isotype IgG and no antibody controls were included. Two independent experiments were performed in duplicates. Data shows the mean ± SEM from three independent experiments. Significance was determined by one-way ANOVA with Dunnett's post-test compared to isotype control. (*P < 0.05, **P < 0.01, ***P < 0.001). **B) CryoEM micrograph of the FabC10 when complexed with DENV2_NGC virus can inhibit viral fusion.** Top panel, control uncomplexed DENV2 particles at various pH conditions. At pH 8.0→pH8.0 and pH 8.0→pH 6.5, virus particles are largely smooth surfaced. At pH 8.0→pH 5.0, the virus seems to have a smaller diameter and a spiky surface, the virus particles have also aggregated together. Bottom panel, when complexed

with Fab C10, the virus particles at all pH conditions appears spiky, indicating Fab binding. No aggregation was detected at any pH conditions. At pH 8.0→pH 5.0, the Fab:DENV2 particles did not fall apart like the uncomplexed DENV2 at the similar pH condition. Scale bar is 500 Å.

Figure 2: Mapping the Fab C10-ZIKV epitope-paratope interface by HDXMS. A) Deuterium exchange difference plot (t=1 min) (Fab C10-ZIKV minus free ZIKV) for ZIKV E-protein peptides. Each point denotes a pepsin fragment peptide of ZIKV E-protein displayed from the N to C-terminus. A positive difference indicates increased exchange in the Fab C10-bound state, a negative difference indicates protection from deuterium exchange in the Fab C10-bound state. Significance threshold for differences in deuterium exchange (+/- 0.5 Da) is indicated as dashed red lines. Standard errors in deuterium uptake for each peptide are shaded green. Domain organization of ZIKV E-protein is indicated below the difference plot. Peptides spanning C10 epitopes are indicated in blue region. **B)** Differences in deuterium exchange between Fab C10:ZIKV complex and ZIKV mapped onto the cryoEM structure of Fab C10:ZIKV complex (PDB ID: 5H37). **C)** Deuterium exchange differences (as per key) mapped onto the whole ZIKV particle from cryoEM structure of Fab C10:ZIKV complex (PDB ID: 5H37). Black triangle indicates an asymmetric unit of ZIKV.

Figure 3: Saturating Fab C10 binding induces particle-wide increased deuterium exchange in DENV2. A) Deuterium exchange difference plot (t=1 min) (Fab C10:DENV2 minus free DENV2) of DENV2 E-protein peptides. A positive difference indicates increased exchange in the Fab C10-bound state, a negative difference indicates protection from deuterium exchange in the Fab C10-bound state. Each point denotes a pepsin fragment peptide of DENV2 E-protein displayed from the N to C-terminus. Significance threshold for differences in deuterium exchange (+/- 0.5 Da) are indicated as dashed red lines. Domain organization of E-protein is illustrated below the difference plot. Peptides spanning C10 epitopes are indicated in blue region. Deuterium exchange difference plot for **B)** heavy chain and **C)** light chain peptides with corresponding heavy and light chain CDRs indicated. Standard errors for each peptide are in purple. **D)** Deuterium exchange differences between Fab C10:DENV2 and DENV2 at 28 °C mapped onto the cryoEM structure of E-protein dimer from DENV2 (PDB ID: 3J27). One E-protein protomer is shaded gray. **E)** Deuterium exchange differences (t=1 min) between free C10 Fab and C10:DENV2 in

C10 onto the cryoEM structure of the C10 fragment (PDB ID: 5H37). The C10 heavy and light chain and their corresponding epitope footprints on sE-protein dimer are indicated by dashed cyan and pink circles, respectively. **F)** Mass spectra (Relative intensity (%) versus m/z) of deuterium exchanged (Dex t = 1 min) representative peptides spanning sites showing spectral widening as denoted by numbers of spectral peaks indicated in free DENV2 and Fab C10-bound states. Mass spectra for a representative peptide (31-42) not showing any broadening of peak width upon Fab C10 binding. Indicated peptides mapped onto the structure of the E-protein dimer. **G)** Deuterium exchange differences (as per key) mapped onto the whole DENV2 particle (PDB ID: 3J27)) with regions showing increases in exchange in red. A raft unit is indicated by black rhombus.

Figure 4: Mapping Fab C10 epitopes and paratopes at sub-saturating Fab C10 concentrations reveal heterogeneity in C10 epitopes on DENV2. Differences in deuterons after 1 min of deuterium exchange molar ratio of Fab C10:Eprotein **A)** 1:3 (orange) or **C)** 2:3 (grey) to uncomplexed DENV2 at 28 °C are represented on a difference plot. Domain organization of E-protein are shown below the difference plot. Significance threshold for differences in deuterium exchange (+/- 0.5 Da) are indicated as dashed red lines. Standard error for each peptide is indicated by overlapping shaded regions along the X-axis colored as denoted by the legend key. Peptides spanning C10 epitopes are indicated in blue region. Differences in deuterium exchange in E-protein peptides in **B)** 1:3 or **D)** 2:3 molar ratio of Fab C10:E protein on DENV2 are mapped onto the cryoEM structure of an E-dimer (PDB ID: 3J27). An E-protein protomer is in shaded in yellow. C10 epitope residues identified by cryoEM are represented by spheres. **Increased dynamics of DENV2 E protein units with increasing Fab C10 binding. E)** Mass spectra (Relative intensity (%) versus m/z) of representative peptides from DENV2 E- and M-proteins at different molar ratios of 1:3, 2:3 and 3:3 Fab C10:E-protein on DENV2 after 1 min of deuterium exchange. Black triangles indicate centroid of the mass envelope. Blue and green dashed lines indicate individual deuterium exchanging populations in bimodal isotopic mass envelopes. Difference in deuterium exchange between C10 epitopes and effects of Fab C10 binding when molar ratios of Fab C10:E on DENV are **F)** 1:3, **G)** 2:3 and **H)** 3:3, identified from cryoEM and HDXMS, are mapped onto

the cryoEM structure of DENV2. Fab C10 epitopes are colored blue and effects of Fab C10 binding are represented in shades of red. A raft unit is indicated by black rhombus.

Figure 5: Saturating concentrations of Fab induced distortion of ~60.4% of the DENV2:Fab C10 particles. A) A table showing percentage of number distorted particles in the DENV2:Fab datasets detected after at different steps of the image reconstruction process- after 2D and, also after 3D classifications. The 2D **(B)** and 3D **(C)** class averages of the DENV2:Fab C10 particles at different Fab:E protein molar ratios. Classes with distorted particles are boxed in red. At Fab:E molar ratios of 1:3, 2:3 and 3:3 at 28^{o}C, there are 0%, 3% and 60.4% distorted particles, respectively.

Figure 6: CryoEM map of the Fab C10:DENV2 complexes at Fab C10:E molar ratio of 1:3, 2:3 and 3:3 to 3,1 Å, 3.3 Å and 3.6 Å, respectively. A) Surface representation of the cryoEM map. Densities corresponding to the E-protein layer and fabs are colored in yellow and red, respectively. Black triangle indicates an asymmetric unit and the 5-, 3-, 2-fold vertices are labeled. **B)** Zoom-in views of the fitted molecule into the density map (grey transparent mesh). **C) CryoEM maps of Fab C10:DENV2 complex displayed at different contour levels.** Densities corresponding to the E-protein layer and fabs are colored in yellow and red, respectively. Black triangle indicates an asymmetric unit. In molar ratio of 1Fab:3E, 2Fab:3E, densities of the Fabs bound to L2 dimers are observe but not those on the I2 dimers (black arrow). **D) Table of the Fab C10 occupancies on the three individual epitopes of an asymmetry unit of the cryoEM Fab:DENV maps at different Fab:E molar ratios.** Occupancies are calculated by: average map value of (Fab÷E dimer) ×100%. **E)** E protein dimer with peptides of increased dynamics (detected by HDXMS) colored in red and the residues forming the C10 epitope (identified by cryoEM) colored as green spheres. **F) The C10 epitopes (circled by red dotted line) in an E protein raft.** The C10 epitopes identified by using a distance cutoff of 8 Å between the Cα chains of the Fab and the E protein. The Fab molecules bind to both ends of each E protein dimer (L2 and I2). The E protein molecules A, B and C in one raft are coloured in pink, yellow and dark green, respectively, while the E proteins in the neighbouring rafts are in grey. There are three individual C10 epitopes within an asymmetric unit - two of which are binding to the two ends of a L2 dimer

(green:pink dimer) – one around the 5-f vertex and another near the 3-f vertex, while the other epitope is on the I2 dimer (yellow:yellow dimer). The epitope residues within the intra-dimer interface are shown as light blue spheres, while the inter-dimer and inter-raft interfaces as dark blue and red spheres, respectively. **G) The fit of E protein and Fab C10 into the cryoEM map of the Fab:DENV2 (molar ratio 3Fab:3E).** The Zoom-in panel shows the distance of the interactions (dotted red lines) between Fab and E dimer. The densities of variable regions of Fab heavy and light chains are coloured as magenta and cyan mesh, respectively, the that of the E protein mols A and C' of the L2 dimer is colored as lime green and yellow mesh, respectively.

Figure 7: Cryo EM structure of DENV2 :F(ab')$_2$. A) the micrographs of the DENV2 complexed with bivalent antibody IgG and F(ab')$_2$. The micrograph showed bivalent antibody aggregates virus. **B) the final resolution map of DENV2 :F(ab')$_2$ is determined to 3.5 Å.** The Fab density appeared at quite low contour level as indicated by the low occupancy of the F(ab')$_2$. **C) Localised reconstruction of the asymmetry units showed a special class which just Fab density appear on the 3-fold.** The E protein F(ab')$_2$ structure fit well to the map, the distance between 2 Fab is 40 Å which is a reasonable for pairing from one F(ab')$_2$ D**) The binding model of bivalent antibody.** Bivalent antibody binds across the 3-fold. The structure shows as surface. And the E protein (the raft bound with F(ab')$_2$) and the heavy chain and light chain are colored as cyan (salmon), light green and rosy brown, respectively.

The Legend of Supplementary Information

Figure S1. Arrangements of E-proteins on mature DENV particles and Sequence coverage map of pepsin proteolysis peptides of E-protein and Fab. Related to Figure 2,3,4

A) Arrangements of E-proteins on mature DENV particles. Six E-proteins arranged as three parallel dimers (blue, red and yellow) in a rhombic raft unit are shown in cartoon. E-protein at the five-fold, two-fold and three-fold vertices are labelled A, B and C, respectively. The blue and yellow dimers are also annotated as L2 dimers and the red dimer is annotated the I2 dimer. The three types of quaternary interactions interfaces namely, inter-raft, interdimer and intradimer interactions are indicated in black, green and cyan dashed lines respectively. **B)** Sequence

coverage map of pepsin proteolysis peptides of whole ZIKV E-protein. Each orange line represents a single pepsin proteolysis peptide listed from the N to C-terminus. **C)** Sequence coverage map of pepsin proteolysis peptides of the heavy and light chain of Fab C10 Fab fragments and the DENV2 structural proteins C-, E- and M-proteins. Pepsin fragmentation peptides the heavy and light chain of Fab C10 are represented in cyan and pink bars respectively and DENV2 C-, E- and M-proteins are represented in red, blue and yellow bars respectively. Each line represents a single pepsin proteolysis peptide listed from the N to C-terminus.

Figure S2. Epitope and paratope mapping of Fab C10-ZIKV and Fab C10-recombinant sE-protein complex by HDXMS. Related to Figure 2 **A)** Deuterium exchange difference plots (t =1 min) (Fab C10-ZIKV minus free Fab C10) of B) heavy and **B)** light chain peptides of C10 Fab. Standard errors in deuterium uptake for each peptides are shaded green. **C)** Deuterium exchange differences in C10 heavy and light chains mapped onto Fab C10. The C10 heavy and light chain and their corresponding epitope footprints on sE-protein dimer are indicated by dashed cyan and pink circles, respectively. C10 Fab showing the peptides showing decreased deuterium exchange with corresponding heavy and light chain CDRs indicated. **D)** Deuterium exchange difference plot (t=1 min) (Fab C10:DENV2 minus free DENV2) of DENV2 E-protein peptides. A positive difference indicates increased exchange in the Fab C10-bound state, a negative difference indicates protection from deuterium exchange in the Fab C10-bound state. Significance threshold for differences in deuterium exchange (+/- 0.5 Da) are indicated as dashed red lines. Standard error of deuterium exchange are indicated in blue. Domain organization of sE-protein is shown below the difference plot. **E)** Differences in deuterium exchange in E-protein peptides between Fab C10:sE-protein and uncomplexed sE-protein mapped onto the crystal structure of Fab C10:sE-protein dimer (PDB ID: 4UT9). An E-protein protomer is shaded in grey. Differences in deuterium exchange in FAB C10 **F)** heavy and **G)** light chain peptides between Fab C10-recombinant E-protein and free Fab C10 after 1 min of deuterium exchange are represented in individual difference plots. **H)** Differences in deuterium exchange in Fab C10 heavy and light chain peptides between Fab C10:sE-protein and uncomplexed C10 mapped onto the crystal structure of C10 fab fragment (PDB ID: 4UT9). The Fab C10 heavy and light chain and their corresponding epitope footprints on sE-protein dimer are indicated by dashed cyan and pink circles, respectively. Epitope and paratope residues identified by cryoEM were defined based on a ≤ 4 Å distance cutoff between Fab C10 heavy and light chains and

DENV E-protein (clustered into salt bridges (≤ 4 Å) and H-bonding interaction (≤ 3.5 Å) respectively (Rouvinski et al. (2015) Nature).

Figure S3. Deuterium exchange difference plots of at 3 different ratios of Fab C10 : E-proteins and Serotype-specific deuterium exchange heat map of DENV2 and ZIKV. Related to Figure 3 Deuterium exchange difference plot of A) 1 Fab: 3 E-proteins, B) 2 Fab: 3 E-proteins and C) 3 Fab : 3 E-proteins. Difference in deuterons after 1 min of deuterium exchange between free C10 Fab and 1 Fab: 3 E-proteins (orange) or 2 Fab: 3 E-proteins (grey) in C10 **D)** heavy and **E)** light chain peptides are represented as individual difference plots. Each point represents a single pepsin proteolysis peptide of Fab C10 heavy and light chains listed from N to C-terminus. Difference in deuterons (Y-axis) plotted against peptides (X-axis). The significance threshold for deuterium exchange differences (0.5 Da) are shown as a red dashed line. Standard error for each peptide is shown as orange and grey shaded regions along the X-axis as per key. **F)** Differences in deuterium exchange in the Fab C10 heavy and light chain peptides between 1 Fab: 3 E-proteins (orange) or 2 Fab: 3 E-proteins (grey) and C10 are mapped onto the cryo-EM structure of the C10 fragment (PDB ID: 5H37). **G)** RFU after 1 min of deuterium exchange at 28 °C is mapped onto whole viral particles in a color coded gradient scale on DENV2 (PDB ID: 3J27) and ZIKV (PDB ID: 5IZ7). Regions with no peptide coverage are white. Each E-protein monomer is outlined (consisting of 6 monomers). E-protein units adjacent to the five-fold, two-fold and three-fold vertices are labelled A, B and C respectively. **Insets:** RFU after 1 min of deuterium exchange at 28 °C mapped onto a unit of E-protein dimer from DENV2 and ZIKV. Serotype-specific deuterium exchange heat map of DENV2 is adapted from our previous study (Lim et al., 2017).

Figure S4. Deconvolution of bimodal mass spectral envelopes for deuterium exchange in three peptides at three C10 concentrations. Related to Figure 4 Deconvolution of bimodal mass spectral envelopes for deuterium exchange in A) E-peptide 83-107 B) E-peptide 238-260 and C) M-peptide 33-47) at three C10 concentrations. The deconvolved isotopic envelopes for the low exchanging (left envelope) and high exchanging (right envelope) populations are green and red respectively. Deconvolution was carried out using HDExaminer version 3.2 (Sierra Analytics, Modesto CA).

Figure S5. Local resolution plot mapped onto an asymmetric unit of the Fab C10:DENV2 complex (Molar ratio of 3Fab:3E) and the model-to-map FSC. Related to Figure 6

A) Local map resolution was estimated with ResMap. The E protein raft of the Fab C10:DENV2 complex is obtained by localized reconstruction method. The resolution range is shown from 3.5 to 5.0. **B)** B-factor distribution on the L2 and I2 E protein dimers. The C chains are colored according to their B-factors.

Figure S6. The data processing workflow. Related to Figure 6 and Figure 7

The cryo-EM processing workflow of **A)** 1 Fab: 3 E-proteins at 28℃, **B)** 2 Fab : 3 E-proteins at 28℃, and **C)** 3 Fab : 3 E-proteins at 28℃. **D)** DENV2_NGC complexed with F(ab')$_2$.

Figure S7. Localized reconstruction of DENV2:F(ab')2 map. Related to Figure 7

A) Classification of the localized reconstructions of regions around an E protein raft (C1 symmetry) shows three structural classes, Class I-III. Class I: 15 % has one F(ab')$_2$ binding to two E dimers across two 3-f vertices. Class II: 54% of the raft have very low F(ab')$_2$ densities distributed evenly to the 5-, 3-, and 2-fold vertices and Class III (29% of the raft) with no F(ab')$_2$ bound. **B) Comparison of 3-fold Fab densities between DENV2:F(ab')$_2$ and DENV2:Fab cryoEM maps.** In the **DENV2:F(ab')$_2$** map, the distance between the two Fab constant region is approximately 40 Å suggesting these two Fab densities belongs to one F(ab')$_2$ binding to two E dimers across two 3-f vertices. In the DENV2:Fab cryoEM map, the distance between the constant regions of the two Fabs binding to the same 3-f vertices, are further apart (~100 Å). **C) Fitting of the Fabs (from** F(ab')$_2$) **into its corresponding weak densities around 5-f and 2-f vertices.** Left panel**:** the distance between Fabs from two neighbouring 5-fold is 66 Å while that between 5-f and 2-f is 56 Å. This suggests the Fabs if bound are unlikely to derive from one F(ab')$_2$. Right panel: side view of the Fab structure fitted into its corresponding density around the 5-f vertices **D) Model of a IgG cross binding to two different virus particles that will lead to aggregation of the viruses. W**hen a Fab arm of an IgG bind to either 5-f or 2-f vertices, the other Fab arm will not be able to engage any epitope within the same viral particle and hence this Fab arm will likely bind to other viral particles causing aggregation.

Table S1. Summary of DENV2 E-protein epitope residues for Fab C10 and nature of contacts. Related to Figure 6 C10 epitopes residues on DENV2 E-proteins identified from previous structural studies. (Rouvinski et al., 2015)

Table S2. Occupancy of Fab C10 estimated by Chimera. Related to Figure 7

Table S3 Cryo-EM data collection, refinement and validation statistics. Related to Figure 6 and Figure7

Key resources table

REAGENT or RESOURCE	SOURCE	IDENTIFIER
Antibodies		
Human monoclonal antibody C10	Prof Gavin Screaton (University of Oxford)	N/A
Bacterial and virus strains		
DENV2 New Guinea C (NGC)	The laboratory of Michael Rossmann	N/A
ZIKV H/PF/2013	Prof Michael Diamond (Washington University School of Medicine)	001v-EVA1545
Chemicals, peptides, and recombinant proteins		
Potassium tartrate tetrahydrate	Sigma-Aldrich	217255
polyethylene glycol (PEG 8000)	Sigma-Aldrich	25322-68-3
D_2O	Cambridge Isotope Laboratory Inc.	7789-20-0
titanium dioxide (TiO_2)	Sigma-Aldrich	13463-67-7
Recombinant E protein	This paper	N/A
Critical commercial assays		
qScript cDNA SuperMix	Quantabio	Cat# 95048-100
iQ SYBR Green Supermix	Bio-Rad	Cat# #1708880
Deposited data		
Cryo-EM density map of DENV2:Fab C10 at Molar ratio of 1Fab:3E at 28 ℃	This paper	EMDB: 31677
Coordinates of molecular model of DENV2:Fab C10 at Molar ratio of 1Fab:3E at 28 ℃	This paper	PDB: 7V3F
Cryo-EM density map of DENV2:Fab C10 at Molar ratio of 2Fab:3E at 28 ℃	This paper	EMDB: 31678
Coordinates of molecular model of DENV2:Fab C10 at Molar ratio of 2Fab:3E at 28 ℃	This paper	PDB: 7V3G
Cryo-EM density map of DENV2:Fab C10 at Molar ratio of 3Fab:3E at 28 ℃	This paper	EMDB: 31679
Coordinates of molecular model of DENV2:Fab C10 at Molar ratio of 3Fab:3E at 28 ℃	This paper	PDB: 7V3H
Cryo-EM density map of DENV2:F(ab')$_2$ C10_local map	This paper	EMDB: 31681
Coordinates of molecular model of DENV2:F(ab')$_2$ local map	This paper	PDB: 7V3J
Cryo-EM density map of DENV2:F(ab')$_2$ C10_whole map	This paper	EMDB: 31681
Experimental models: Cell lines		
C6/36 Aedes albopictus mosquito cells	American Type Culture Collection (ATCC)	ATCC® Number: CRL-1660
BHK-21	American Type Culture Collection (ATCC)	ATCC® Number: CCL-10

S2 drosophila cells	This paper	N/A
Oligonucleotides		
qPCR forward primer 5'-CAGGCTATGGCACTGTCACGATG -3'	IDT	N/A
qPCR reverse primer 5'-CCATTTGCAGCAACACCATCTC -3'	IDT	N/A
Gapdh- Forward: 5′-GGCAAGTTCAAAGGCACAGTC-3′	IDT	N/A
Gapdh-Reverse: 5′-CACCAGCATCACCCCATTT-3′	IDT	N/A
Software and algorithms		
Cryosparc	Punjani et al., 2017	https://cryosparc.com/
RELION	Scheres, 2012	https://www2.mrc-lmb.cam.ac.uk/relion/index.php?title=Main_Page
Chimera	Pettersen et al., 2004	https://www.cgl.ucsf.edu/chimera/
GraphPad Prism 5	GraphPad	https://www.graphpad.com
Phenix.real_space_refine	Afonine et al., 2018	https://www.phenix-online.org
Coot	Emsley and Cowtan, 2004	https://www2.mrc-lmb.cam.ac.uk/personal/pemsley/coot/
DynamX™ HDX Analysis Software	Waters, Milford MA	N/A
HDExaminer version 3.2	Sierra Analytics, Modesto CA	N/A

Figure 4

Click here to access/download;Figure;Figure4.tif

Figure 4. Mapping Fab C10 epitopes and paratopes at sub-saturating Fab C10 concentrations reveal heterogeneity in C10 epitopes on DENV2

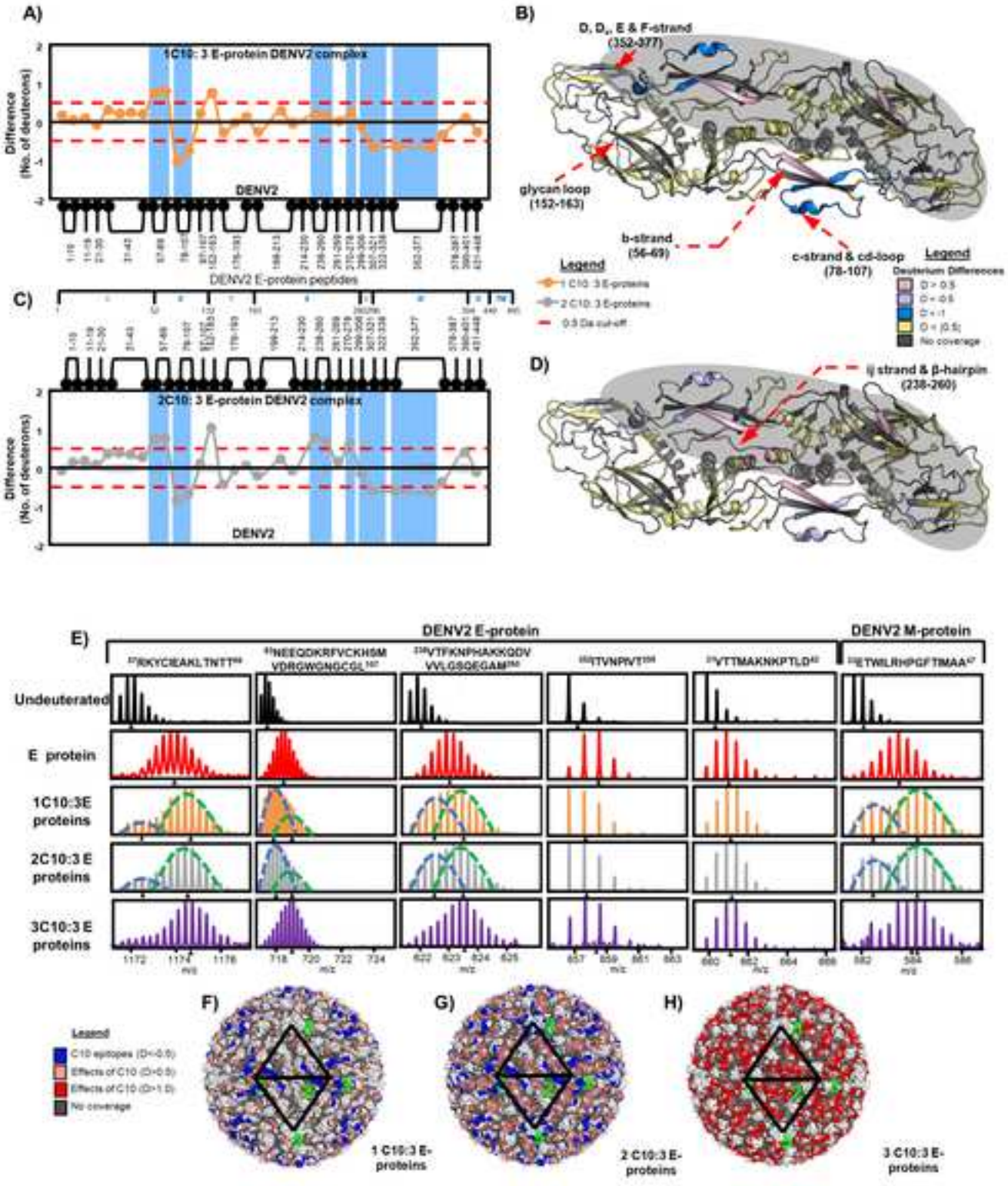

Figure 5. Saturating concentrations of Fab induced distortion of ~60.4% of the DENV2:Fab C10 particles

A)

Molar ratios	Number of DENV2:Fab complex particles detected from 2D and 3D class averageing	Number of distorted particles detected		% total distorted particles detected after both 2D and 3D class averaging	Particles used for image reconstruction.
		After 2D class averaging	After 3D class averaging		
3Fab:3E	141235	38935	46426	60.4	42509
2Fab:3E	112713	3150	0	3	70534
1Fab:3E	177850	0	0	0	109712

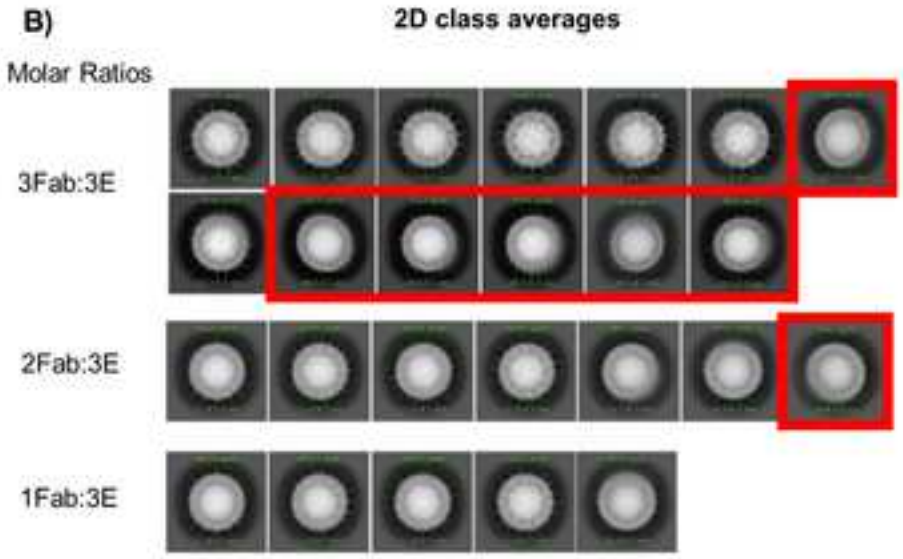

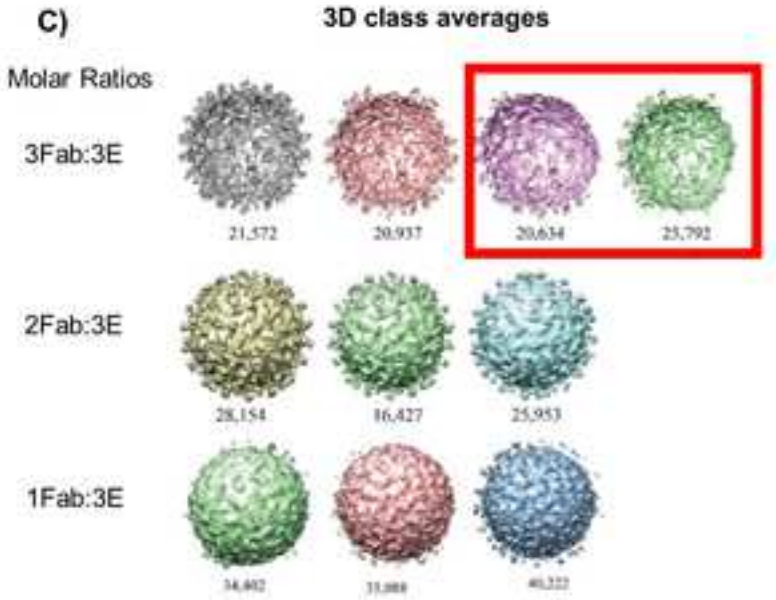

Figure 6

Click here to access/download;Figure;figure6.tif

Figure 6. CryoEM map of the Fab C10:DENV2 complexes at different Fab C10:E molar ratio

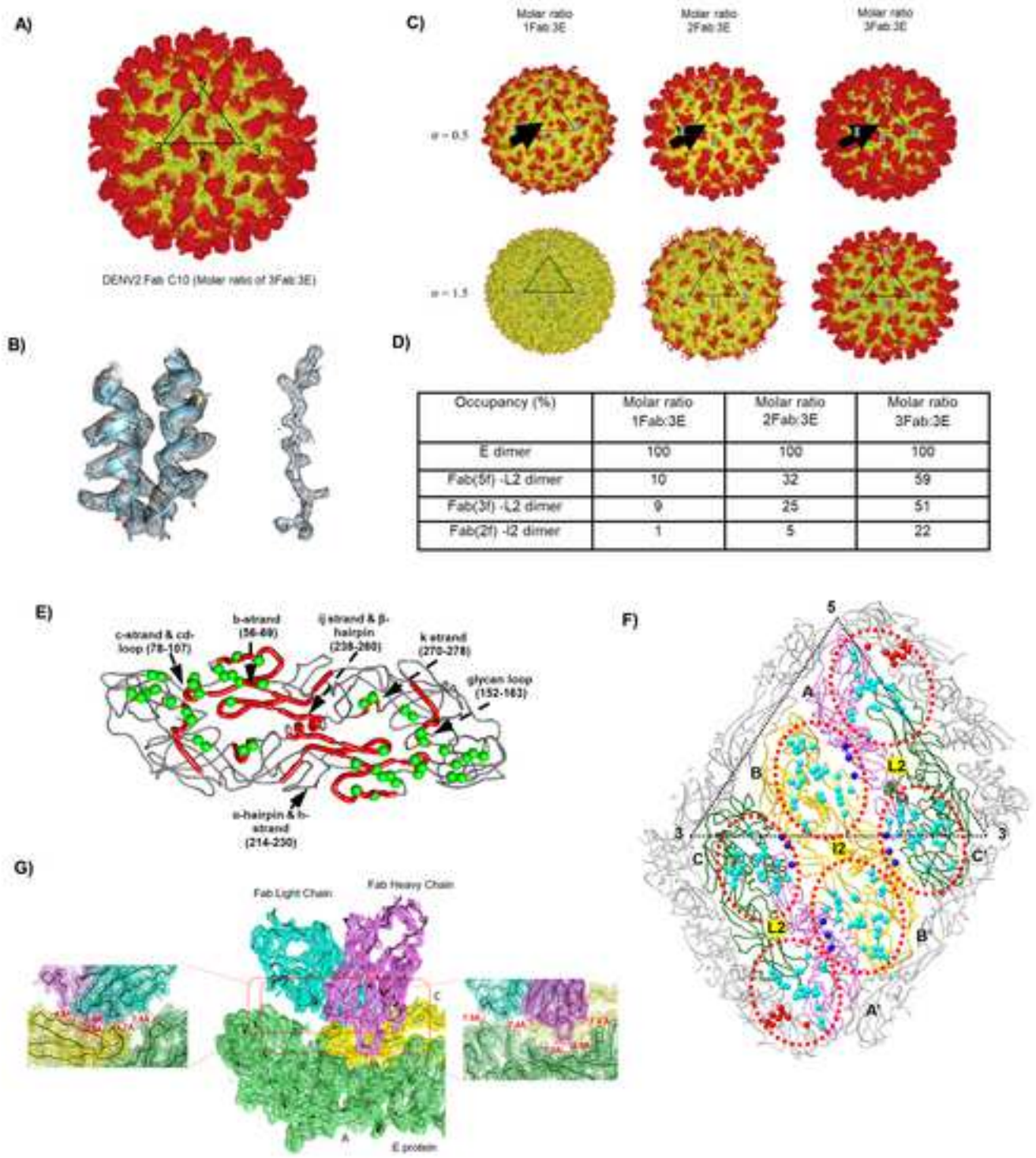

Occupancy (%)	Molar ratio 1Fab:3E	Molar ratio 2Fab:3E	Molar rabo 3Fab:3E
E dimer	100	100	100
Fab(5f) -L2 dimer	10	32	59
Fab(3f) -L2 dimer	9	25	51
Fab(2f) -I2 dimer	1	5	22

Figure 7

Figure 7. Cryo EM structure of DENV2 :F(ab')$_2$

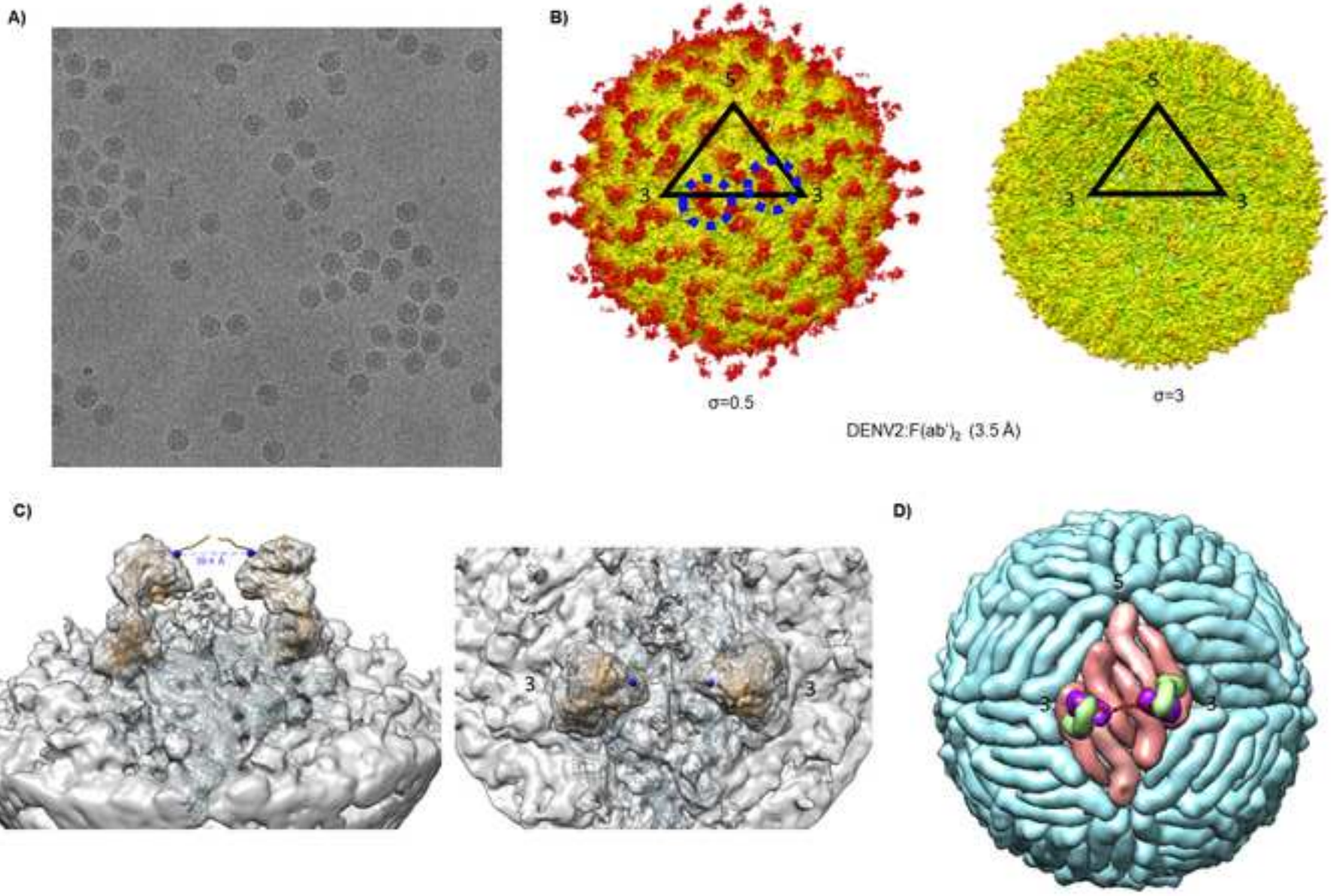

Figure 1

Click here to access/download;Figure;Figure1.tif

Figure 1. The neutralization of antibody C10

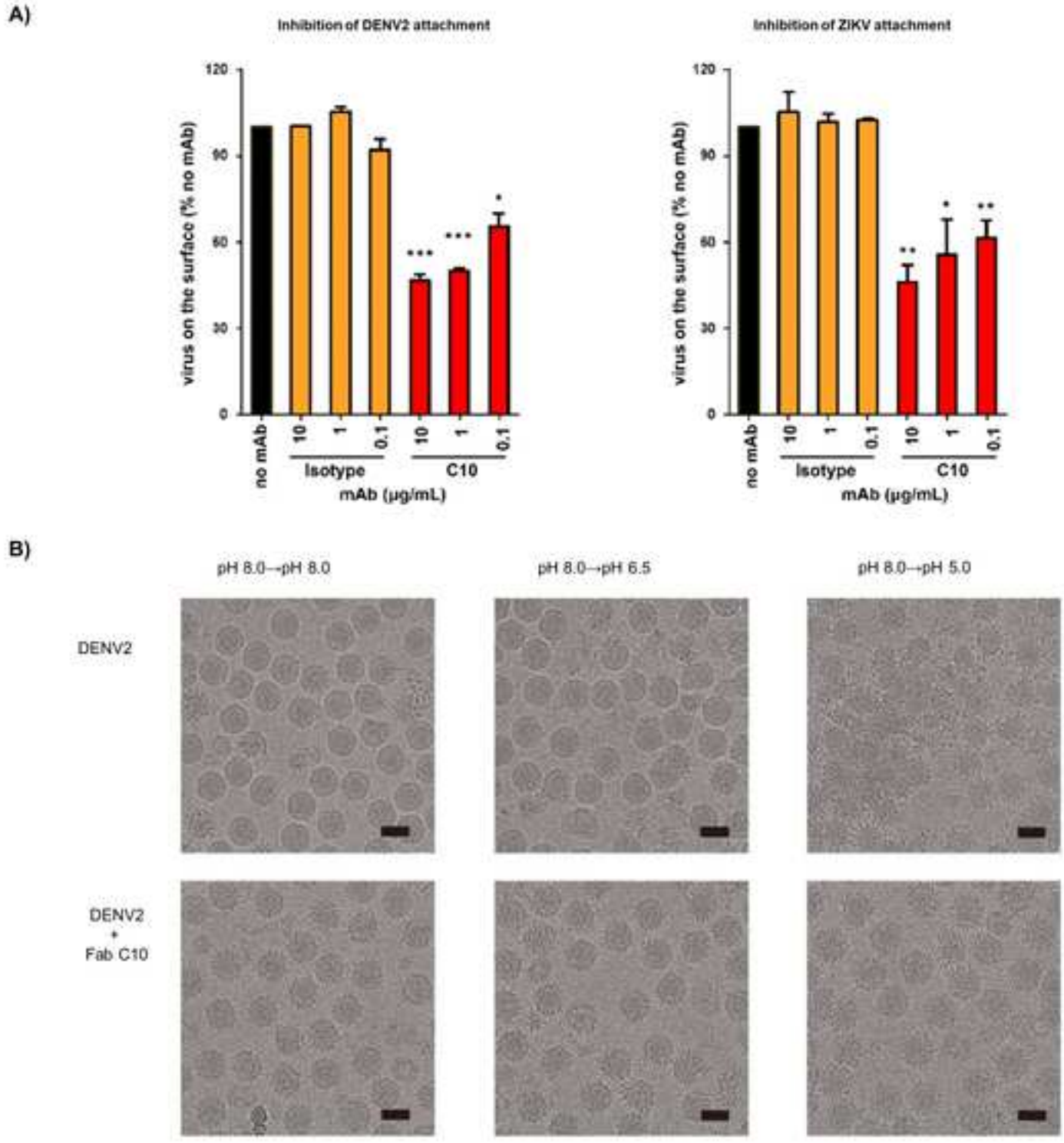

Figure 2. Mapping the Fab C10-ZIKV epitope-paratope interface by HDXMS

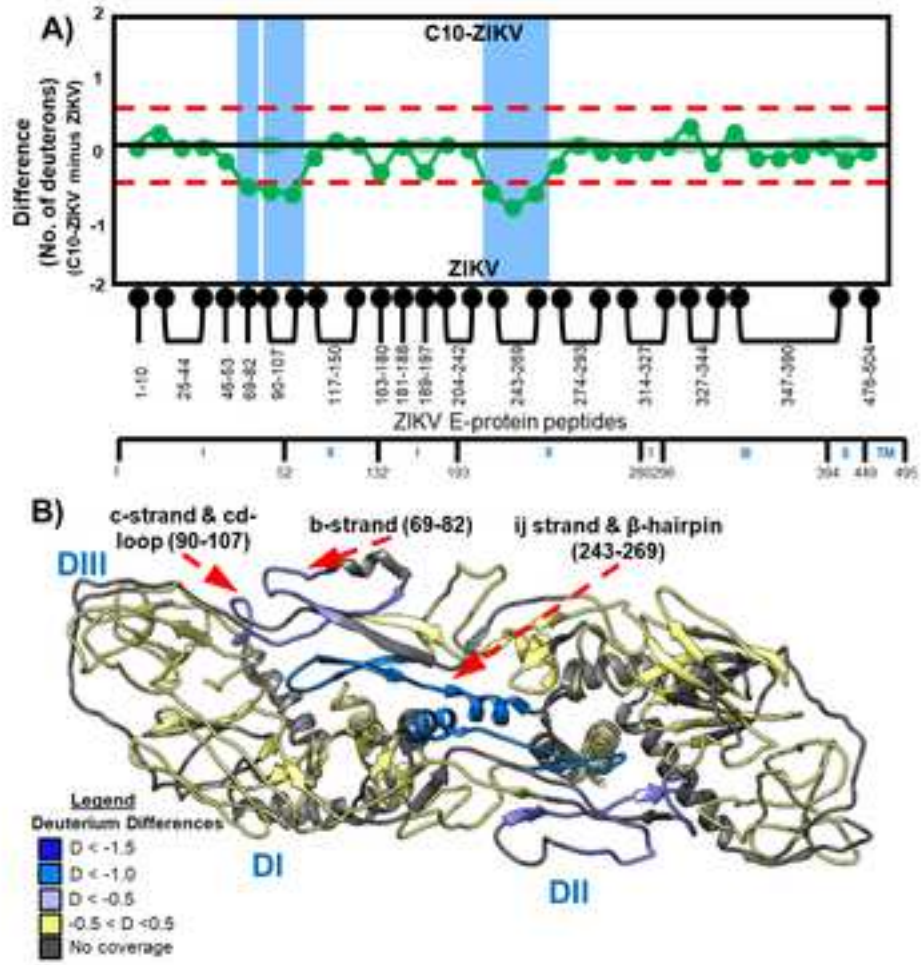

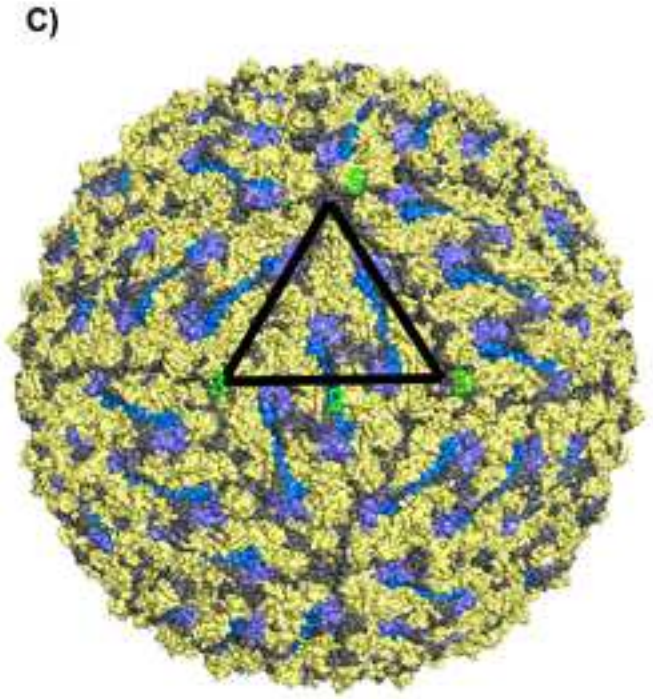

Figure 3

Click here to access/download;Figure;Figure3.tif

Figure 3. Saturating Fab C10 binding induces particle-wide increased deuterium exchange in DENV2

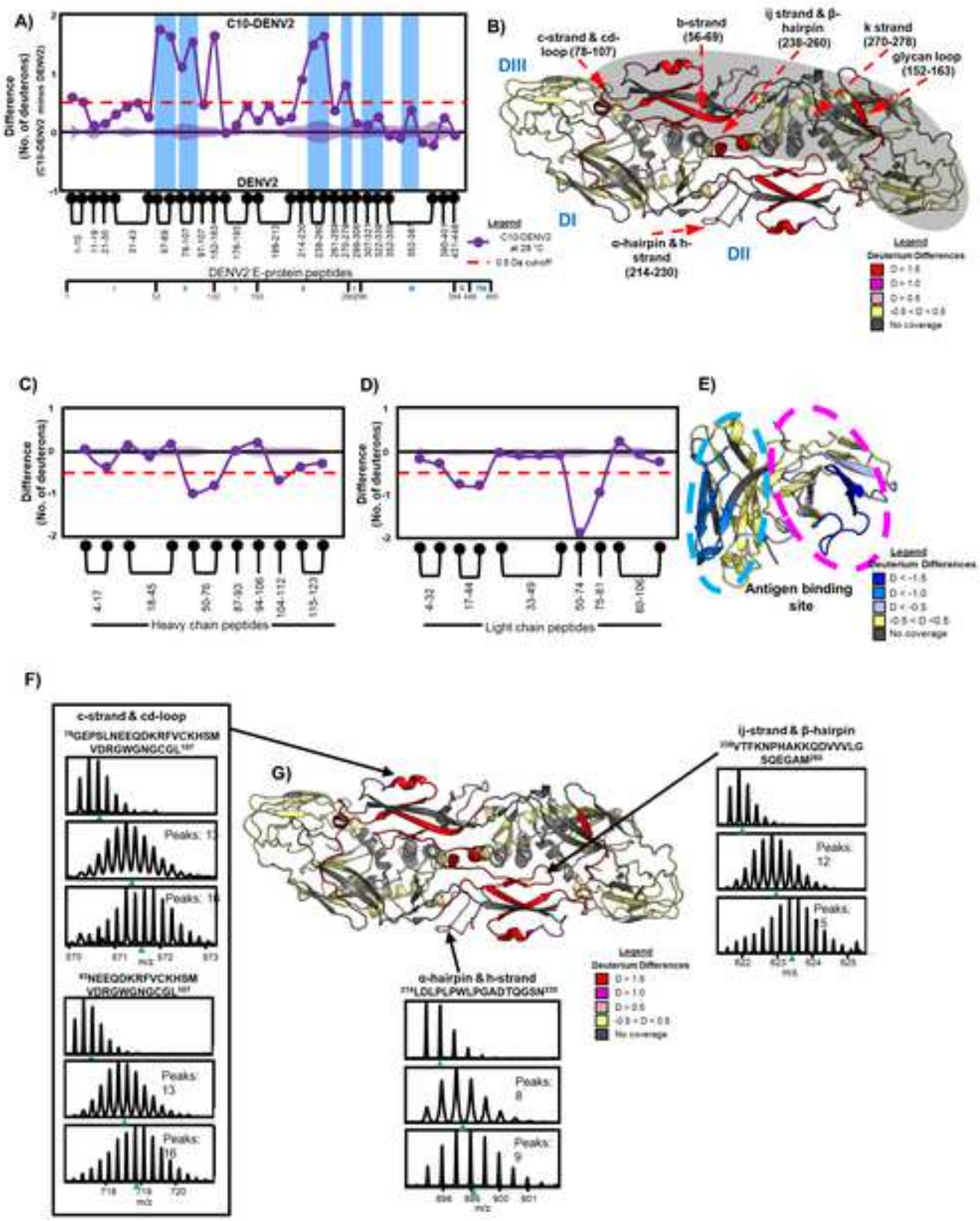

The Legend of Supplementary Information

Figure S1. Arrangements of E-proteins on mature DENV particles and Sequence coverage map of pepsin proteolysis peptides of E-protein and Fab. Related to Figure 2,3,4
A) Arrangements of E-proteins on mature DENV particles. Six E-proteins arranged as three parallel dimers (blue, red and yellow) in a rhombic raft unit are shown in cartoon. E-protein at the five-fold, two-fold and three-fold vertices are labelled A, B and C, respectively. The blue and yellow dimers are also annotated as L2 dimers and the red dimer is annotated the I2 dimer. The three types of quaternary interactions interfaces namely, inter-raft, interdimer and intradimer interactions are indicated in black, green and cyan dashed lines respectively. **B)** Sequence coverage map of pepsin proteolysis peptides of whole ZIKV E-protein. Each orange line represents a single pepsin proteolysis peptide listed from the N to C-terminus. **C)** Sequence coverage map of pepsin proteolysis peptides of the heavy and light chain of Fab C10 Fab fragments and the DENV2 structural proteins C-, E- and M-proteins. Pepsin fragmentation peptides the heavy and light chain of Fab C10 are represented in cyan and pink bars respectively and DENV2 C-, E- and M-proteins are represented in red, blue and yellow bars respectively. Each line represents a single pepsin proteolysis peptide listed from the N to C-terminus.

Figure S2. Epitope and paratope mapping of Fab C10-ZIKV and Fab C10-recombinant sE-protein complex by HDXMS. Related to Figure 2 **A)** Deuterium exchange difference plots (t =1 min) (Fab C10-ZIKV minus free Fab C10) of B) heavy and **B)** light chain peptides of C10 Fab. Standard errors in deuterium uptake for each peptides are shaded green. **C)** Deuterium exchange differences in C10 heavy and light chains mapped onto Fab C10. The C10 heavy and light chain and their corresponding epitope footprints on sE-protein dimer are indicated by dashed cyan and pink circles, respectively. C10 Fab showing the peptides showing decreased deuterium exchange with corresponding heavy and light chain CDRs indicated. **D)** Deuterium exchange difference plot (t=1 min) (Fab C10:DENV2 minus free DENV2) of DENV2 E-protein peptides. A positive difference indicates increased exchange in the Fab C10-bound state, a negative difference indicates protection from deuterium exchange in the Fab C10-bound state. Significance threshold for differences in deuterium exchange (+/- 0.5 Da) are indicated as dashed red lines. Standard error of deuterium exchange are indicated in blue. Domain organization of sE-protein is shown below the difference plot. **E)** Differences in deuterium exchange in E-protein peptides between Fab C10:sE-protein and uncomplexed sE-protein mapped onto the crystal structure of Fab C10:sE-protein dimer (PDB ID: 4UT9). An E-protein protomer is shaded in grey. Differences in deuterium exchange in FAB C10 **F)** heavy and **G)** light chain peptides between Fab C10-recombinant E-protein and free Fab C10 after 1 min of deuterium exchange are represented in individual difference plots. **H)** Differences in deuterium exchange in Fab C10 heavy and light chain peptides between Fab C10:sE-protein and uncomplexed C10 mapped onto the crystal structure of C10 fab fragment (PDB ID: 4UT9). The Fab C10 heavy and light chain and their corresponding epitope footprints on sE-protein dimer are indicated by dashed cyan and pink circles, respectively. Epitope and paratope residues identified by cryoEM

were defined based on a ≤ 4 Å distance cutoff between Fab C10 heavy and light chains and DENV E-protein (clustered into salt bridges (≤ 4 Å) and H-bonding interaction (≤ 3.5 Å) respectively (Rouvinski et al. (2015) Nature).

Figure S3. Deuterium exchange difference plots of at 3 different ratios of Fab C10 : E-proteins and Serotype-specific deuterium exchange heat map of DENV2 and ZIKV. Related to Figure 3 Deuterium exchange difference plot of A) 1 Fab: 3 E-proteins, B) 2 Fab: 3 E-proteins and C) 3 Fab : 3 E-proteins. Difference in deuterons after 1 min of deuterium exchange between free C10 Fab and 1 Fab: 3 E-proteins (orange) or 2 Fab: 3 E-proteins (grey) in C10 **D)** heavy and **E)** light chain peptides are represented as individual difference plots. Each point represents a single pepsin proteolysis peptide of Fab C10 heavy and light chains listed from N to C-terminus. Difference in deuterons (Y-axis) plotted against peptides (X-axis). The significance threshold for deuterium exchange differences (0.5 Da) are shown as a red dashed line. Standard error for each peptide is shown as orange and grey shaded regions along the X-axis as per key. **F)** Differences in deuterium exchange in the Fab C10 heavy and light chain peptides between 1 Fab: 3 E-proteins (orange) or 2 Fab: 3 E-proteins (grey) and C10 are mapped onto the cryo-EM structure of the C10 fragment (PDB ID: 5H37). **G)** RFU after 1 min of deuterium exchange at 28 °C is mapped onto whole viral particles in a color coded gradient scale on DENV2 (PDB ID: 3J27) and ZIKV (PDB ID: 5IZ7). Regions with no peptide coverage are white. Each E-protein monomer is outlined (consisting of 6 monomers). E-protein units adjacent to the five-fold, two-fold and three-fold vertices are labelled A, B and C respectively. **Insets:** RFU after 1 min of deuterium exchange at 28 °C mapped onto a unit of E-protein dimer from DENV2 and ZIKV. Serotype-specific deuterium exchange heat map of DENV2 is adapted from our previous study (Lim et al., 2017).

Figure S4. Deconvolution of bimodal mass spectral envelopes for deuterium exchange in three peptides at substoichiometric C10 concentrations. Related to Figure 4 Deconvolution of bimodal mass spectral envelopes for deuterium exchange in A) E-peptide 83-107 B) E-peptide 238-260 and C) M-peptide 33-47). The deconvolved isotopic envelope for the low exchanging (left peak) conformation is green and the higher exchanging (right peak) conformation is red. Deconvolution was carried out using HDExaminer version 3.2 (Sierra Analytics, Modesto CA).

Figure S5. Local resolution plot mapped onto an asymmetric unit of the Fab C10:DENV2 complex (Molar ratio of 3Fab:3E) and the model-to-map FSC. Related to Figure 6

A) Local map resolution was estimated with ResMap. The E protein raft of the Fab C10:DENV2 complex is obtained by localized reconstruction method. The resolution range is shown from 3.5 to 5.0. **B)** B-factor distribution on the L2 and I2 E protein dimers. The C chains are colored according to their B-factors.

Figure S6. The data processing workflow. Related to Figure 6 and Figure 7
The cryo-EM processing workflow of **A)** 1 Fab: 3 E-proteins at 28℃, **B)** 2 Fab : 3 E-proteins at 28℃, and **C)** 3 Fab : 3 E-proteins at 28℃. **D)** DENV2_NGC complexed with F(ab')$_2$.

Figure S7. Localized reconstruction of DENV2:F(ab')2 map. Related to Figure 7
A) Classification of the localized reconstructions of regions around an E protein raft (C1 symmetry) shows three structural classes, Class I-III. Class I: 15 % has one F(ab')$_2$ binding to two E dimers across two 3-f vertices. Class II: 54% of the raft have very low F(ab')$_2$ densities distributed evenly to the 5-, 3-, and 2-fold vertices and Class III (29% of the raft) with no F(ab')$_2$ bound. **B) Comparison of 3-fold Fab densities between DENV2:F(ab')$_2$ and DENV2:Fab cryoEM maps.** In the **DENV2:F(ab')$_2$** map, the distance between the two Fab constant region is approximately 40 Å suggesting these two Fab densities belongs to one F(ab')$_2$ binding to two E dimers across two 3-f vertices. In the DENV2:Fab cryoEM map, the distance between the constant regions of the two Fabs binding to the same 3-f vertices, are further apart (~100 Å). **C) Fitting of the Fabs (from** F(ab')$_2$) **into its corresponding weak densities around 5-f and 2-f vertices.** Left panel**:** the distance between Fabs from two neighbouring 5-fold is 66 Å while that between 5-f and 2-f is 56 Å. This suggests the Fabs if bound are unlikely to derive from one F(ab')$_2$. Right panel: side view of the Fab structure fitted into its corresponding density around the 5-f vertices **D) Model of a IgG cross binding to two different virus particles that will lead to aggregation of the viruses. W**hen a Fab arm of an IgG bind to either 5-f or 2-f vertices, the other Fab arm will not be able to engage any epitope within the same viral particle and hence this Fab arm will likely bind to other viral particles causing aggregation.

Table S1. Summary of DENV2 E-protein epitope residues for Fab C10 and nature of contacts. Related to Figure 6 C10 epitopes residues on DENV2 E-proteins identified from previous structural studies. (Rouvinski et al., 2015)

Table S2. Occupancy of Fab C10 estimated by Chimera. Related to Figure 7

Table S3 Cryo-EM data collection, refinement and validation statistics. Related to Figure 6 and Figure7

Figure S4. Deconvolution of bimodal mass spectral envelopes for deuterium exchange in three peptides at substoichiometric C10 concentrations. Related to Figure 4

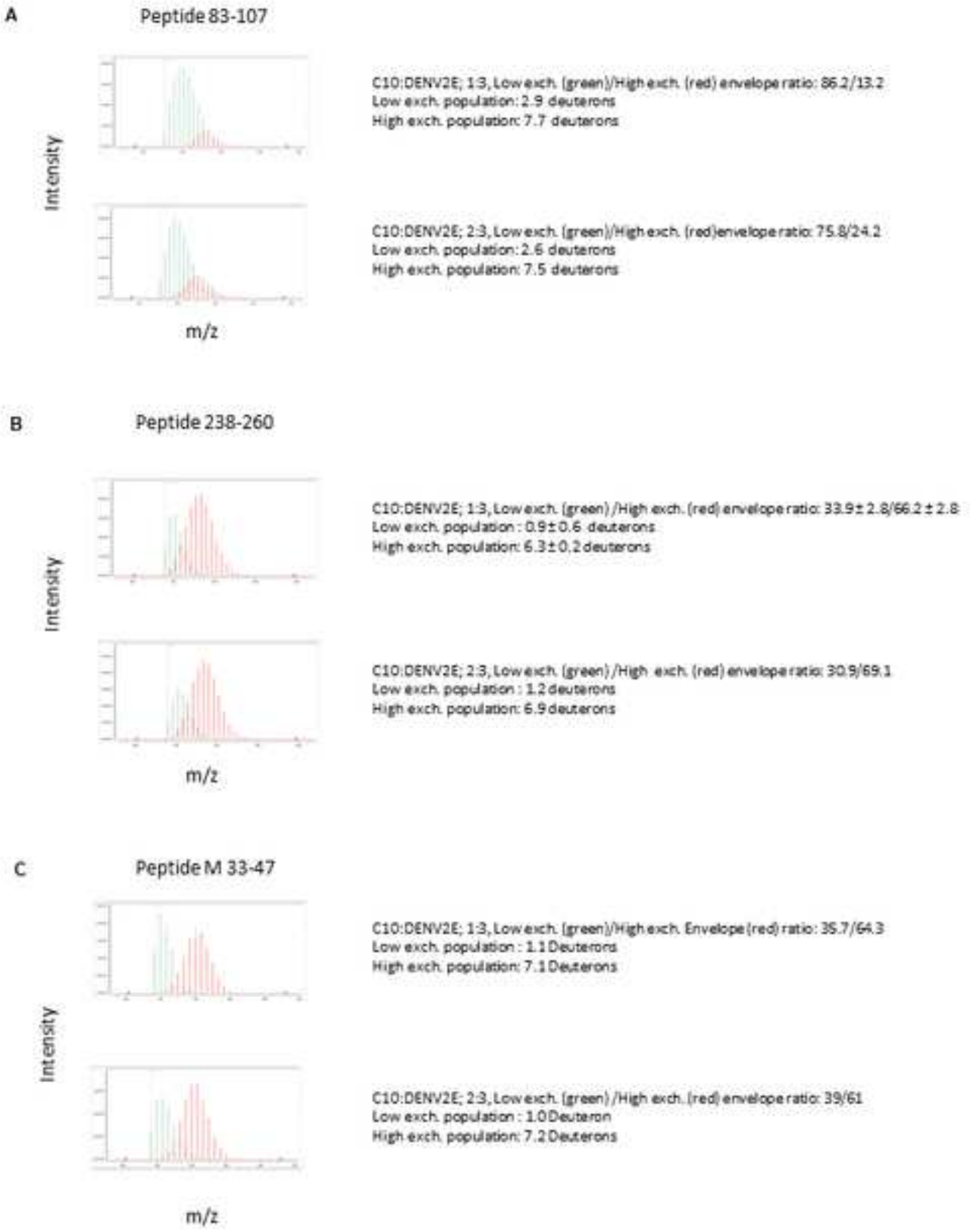

Figure S6. The data processing workflow. Related to Figure 6 and Figure 7

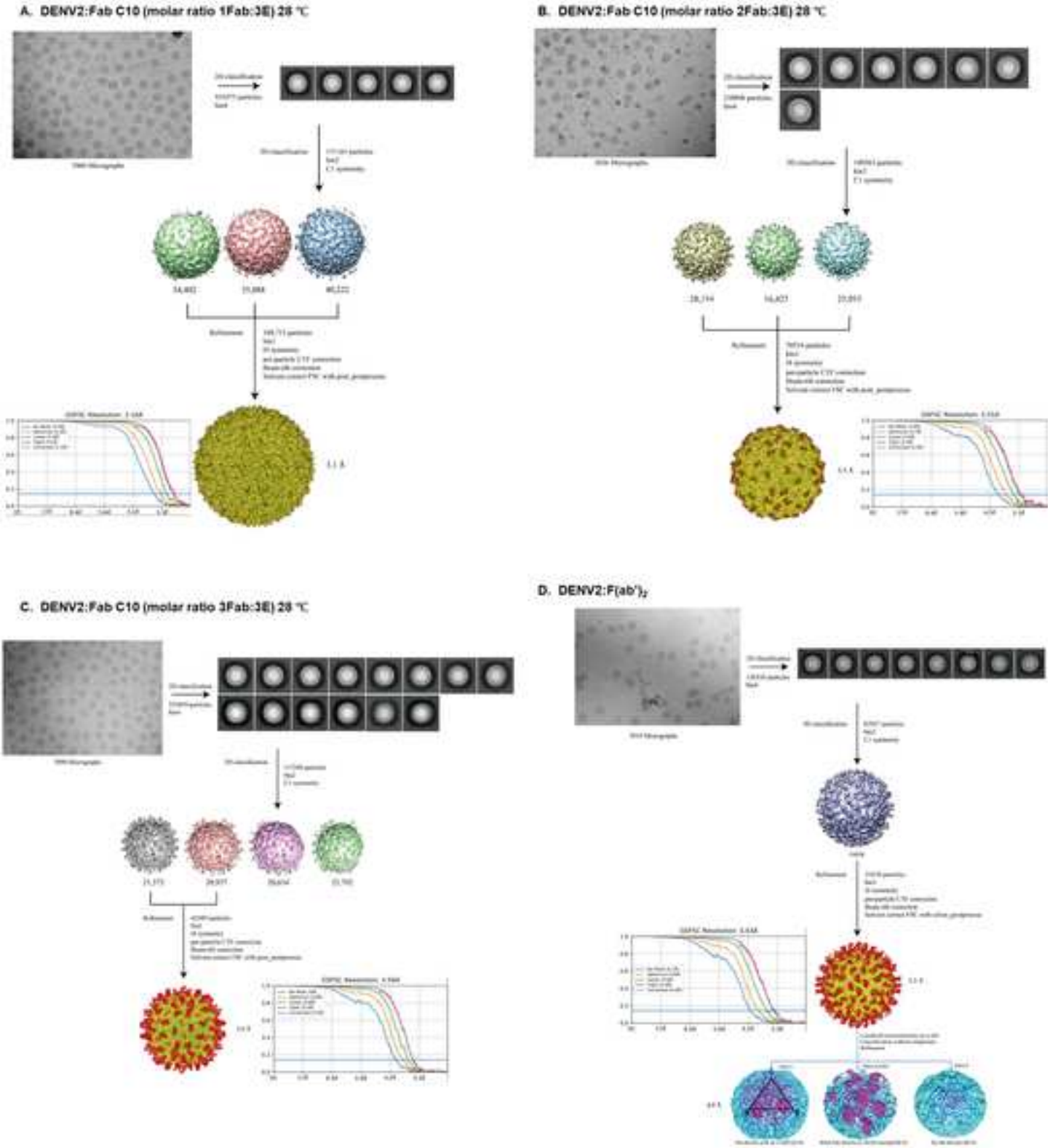

Figure S7. Localized reconstruction of DENV2:F(ab')$_2$ map. Related to Figure 7

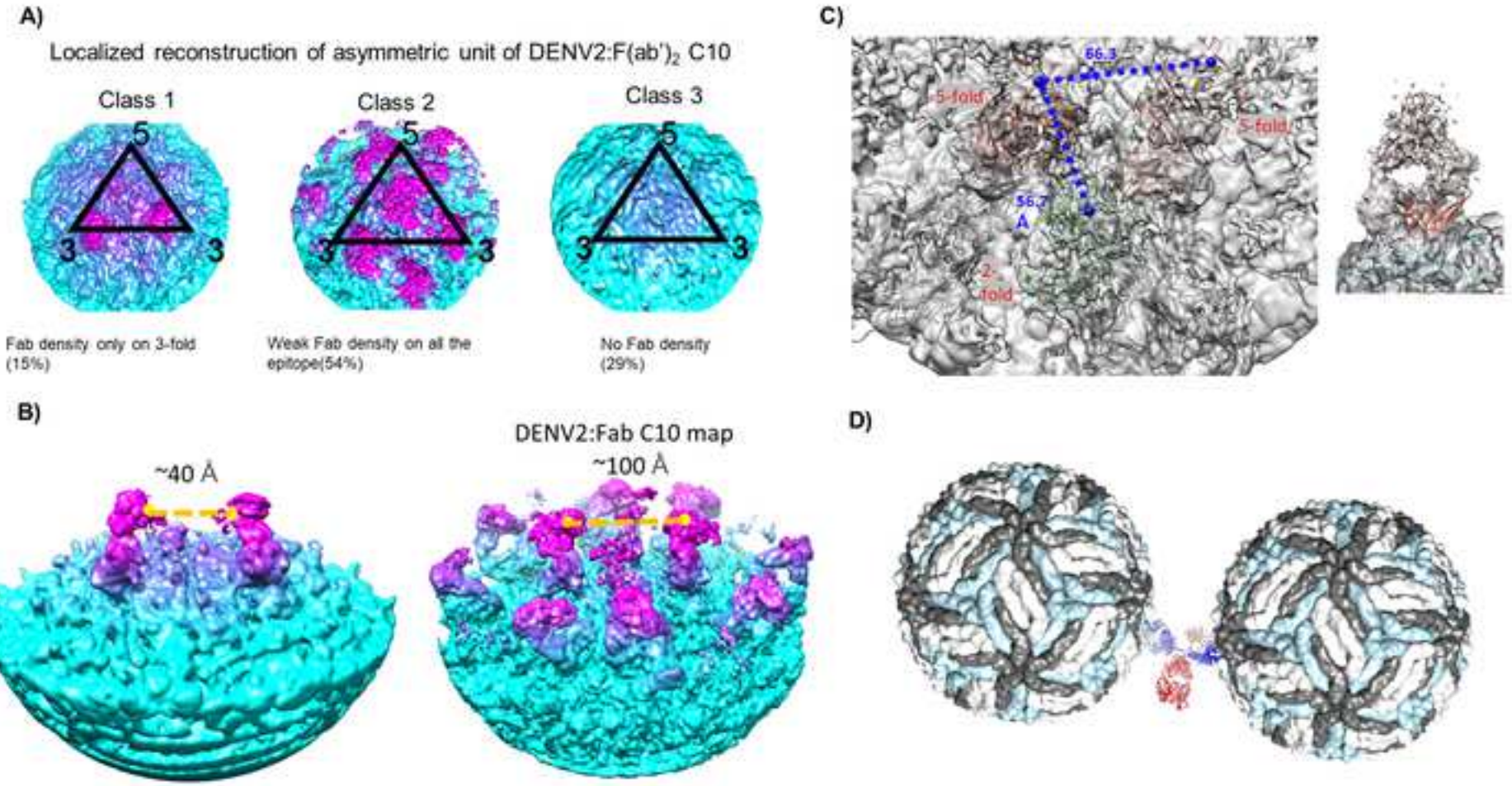

Table S1. Summary of DENV2 E-protein epitope residues for Fab C10 and nature of contacts. Related to Figure 6

Residue No.	Main chain contacts	Side chain contacts	Glycosylation contacts
44		44	
45	45		
67			67
71		71	
72	72		
81	81		
84		84	
104	104		
310		310	
323		323	
362	362		

Table S2. Occupancy of Fab C10 estimated by Chimera. Related to Figure 7

Occupancy (%)	$F(ab')_2$
E dimer	100
Fab(5f) -L2 dimer	8
Fab(3f) -L2 dimer	10
Fab(2f) -I2 dimer	6

Table S3 Cryo-EM data collection, refinement and validation statistics. Related to Figure 6 and Figure 7

	DENV2:Fab C10 Molar ratio (1Fab:3E) 28℃ (EMDB-31677) (PDB 7V3F)	DENV2:Fab C10 Molar ratio (2Fab:3E) 28℃ (EMDB-31678) (PDB 7V3G)	DENV2:Fab C10 Molar ratio (3Fab:3E) 28℃ (EMDB-31679) (PDB 7V3H)	DENV2:F(ab')$_2$-local (EMDB-31681) (PDB 7V3J)
Data collection and processing				
Microscope	FEI Titan Krios	FEI Titan Krios	FEI Titan Krios	FEI Titan Krios
Camera	Gatan K3	Gatan K3	Gatan K3	Gatan K3
Magnification	64,000 X	64,000 X	64,000 X	64,000 X
Voltage (kV)	300	300	300	300
Electron exposure (e–/Å^2)	25	25	25	25
Defocus range (μm)	-0.8 to -2.0	-0.8 to -2.0	-0.8 to -2.0	-0.8 to -2.0
Exposure rate (e-/A2/sec)	8.74	8.86	8.35	5.73
Number of frames per movie	25	25	25	25
Pixel size (Å)	1.345	1.345	1.345	1.345
Energy filter slit width	20	20	20	20
Automation software	SerialEM	SerialEM	SerialEM	SerialEM
Symmetry imposed	I	I	I	C1
Micrographs used	3960	2836	3090	3819
Total number of extracted particles	355475	238,894	235,059	613,170
Total number of refined particles	171161	115862	117240	613,170

Number of particles in final map	109,712	70,534	42,509	93,432
Map resolution (Å)	3.1	3.3	3.6	4.9
FSC threshold	0.143	0.143	0.143	0.143
Local resolution range (Å)	3.1-3.9	3.1-4.2	3.1-4.7	4.2-8.0
Refinement				
Initial model used (PDB code)	3J27	3J27	3J27	3J27
Refinement package, (resolution cutoff)	Phenix, real-sparc refinement	Phenix, real-sparc refinement	Phenix, real-sparc refinement	Phenix, real-sparc refinement
	(3.1)	(3.3)	(3.6)	(4.9)
Resolution of unmasked and masked reconstructions at 0.5 and 0.143 FSC	Unmasked	Unmasked	Unmasked	Unmasked
	3.1/3.6	3.3/3.4	3.4/5.7	4,2/7.5
	Masked	Masked	Masked	Masked
	3.0/3.2	3.2/3.5	3.2/3.5	4.0/4.8
Map sharpening *B* factor ($Å^2$)	-163	-156.5	-168	-206
Estimated accuracy of translations/rotations	0.1295/0.2784	0.134/0.416	0.123/0.4176	1.442/4.939
Model composition				
Non-hydrogen atoms	13230	16802	18616	33252
Protein residues	1701	2173	2409	4304
Ligands	9	9	15	18
Global CC (CCvol)	0.88	0.85	0.84	0.79
Local CC (CCmask)	0.87	0.84	0.83	0.79

B factors (Å^2)				
Protein	37.31	54.42	44.56	277.22
Ligand	49.26	100.17	61.36	362.35
R.m.s. deviations				
Bond lengths (Å)	0.007	0.005	0.007	0.006
Bond angles (°)	0.886	0.836	0.868	0.953
Validation				
MolProbity score	2.25	2.29	2.35	2.79
Clashscore	12.18	14.51	15.47	42.89
Poor rotamers (%)	0.00	0.05	0.00	0.00
C-beta deviations	0.00	0.00	0.00	0.00
Ramachandran plot				
Favored (%)	85.49	87.18	85.53	84.11
Allowed (%)	14.51	12.77	14.47	15.82
Disallowed (%)	0	0	0	0.07
CaBLAM outliers (%)	9.36	7.36	8.01	9.01
EMRinger score	2.65	2.20	2.39	0.24

Supplemental Figure

Click here to access/download;Supplemental Figure;Figure_S1_amended.tif

Figure S1. Arrangements of E-proteins on mature DENV particles and Sequence coverage map of pepsin proteolysis peptides of E-protein and Fab. Related to Figure 2,3,4